

Filtered density function for large eddy simulation of turbulent reacting flows

P. J. Colucci, F. A. Jaber, and P. Givi

Department of Mechanical and Aerospace Engineering, State University of New York at Buffalo, Buffalo, New York 14260-4400

S. B. Pope

Sibley School of Mechanical and Aerospace Engineering, Cornell University, Ithaca, New York 14853-1301

(Received 16 December 1996; accepted 29 September 1997)

A methodology termed the “filtered density function” (FDF) is developed and implemented for large eddy simulation (LES) of chemically reacting turbulent flows. In this methodology, the effects of the unresolved scalar fluctuations are taken into account by considering the probability density function (PDF) of subgrid scale (SGS) scalar quantities. A transport equation is derived for the FDF in which the effect of chemical reactions appears in a closed form. The influences of scalar mixing and convection within the subgrid are modeled. The FDF transport equation is solved numerically via a Lagrangian Monte Carlo scheme in which the solutions of the equivalent stochastic differential equations (SDEs) are obtained. These solutions preserve the Itô-Gikhman nature of the SDEs. The consistency of the FDF approach, the convergence of its Monte Carlo solution and the performance of the closures employed in the FDF transport equation are assessed by comparisons with results obtained by direct numerical simulation (DNS) and by conventional LES procedures in which the first two SGS scalar moments are obtained by a finite difference method (LES-FD). These comparative assessments are conducted by implementations of all three schemes (FDF, DNS and LES-FD) in a temporally developing mixing layer and a spatially developing planar jet under both non-reacting and reacting conditions. In non-reacting flows, the Monte Carlo solution of the FDF yields results similar to those via LES-FD. The advantage of the FDF is demonstrated by its use in reacting flows. In the absence of a closure for the SGS scalar fluctuations, the LES-FD results are significantly different from those based on DNS. The FDF results show a much closer agreement with filtered DNS results. © 1998 American Institute of Physics. [S1070-6631(98)01402-0]

I. INTRODUCTION

Over the past 30 years since the early work of Smagorinsky,¹ significant efforts have been devoted to large eddy simulation (LES) of turbulent flows.^{2–12} The most prominent model has been the Smagorinsky eddy viscosity closure which relates the unknown subgrid scale (SGS) Reynolds stresses to the local large scale rate of flow strain.¹³ This viscosity is aimed to provide the role of mimicking the dissipative behavior of the unresolved small scales. The extensions to “dynamic” models^{14,15} have shown some improvements. This is particularly the case in transitional flow simulations where the dynamic evaluations of the empirical model “constant” result in (somewhat) better predictions of the large scale flow features.

A survey of combustion literature reveals relatively little work in LES of chemically reacting turbulent flows.^{7,16} It appears that Schumann¹⁷ was one of the first to conduct LES of a reacting flow. However, the assumption made in this work simply to neglect the contribution of the SGS scalar fluctuations to the filtered reaction rate needs to be justified for general applications. The importance of such fluctuations is well recognized in Reynolds averaged procedures in both combustion^{18–20} and chemical engineering^{21–24} problems. Therefore, it is natural to believe that these fluctuations are

also important in LES. McMurtry *et al.*,^{25,26} Sykes *et al.*,²⁷ Liou *et al.*,²⁸ Menon *et al.*,²⁹ Boris *et al.*,³⁰ Fureby *et al.*,^{31,32} Cook *et al.*,^{33,34} Mathey and Chollet,³⁵ Branley and Jones³⁶ and others provide several means of conducting LES of turbulent reacting flows.

Modeling of scalar fluctuations in Reynolds averaged methods has been the subject of broad investigations since the pioneering work of Toor.³⁷ An approach which has proven particularly useful is based on the probability density function (PDF) or the joint PDF of scalar quantities.^{38–41} The systematic approach for determining the PDF is by means of solving the transport equation governing its evolution.⁴² In this equation, the effects of chemical reaction appear in a closed form; this constitutes the primary advantage of the PDF schemes in comparison to other statistical procedures. The use of PDF for LES was suggested by Givi⁷ and its first application is due to Madnia and Givi.⁴³ In this work, the Pearson family of distributions are assumed to characterize PDF of SGS scalars in homogeneous flows under chemical equilibrium conditions. This procedure was also used by Cook and Riley.⁴⁴ The extension of assumed PDF methods for LES of non-equilibrium reacting shear flows is reported by Frankel *et al.*⁴⁵ While the generated results are encouraging, they do reveal the need for more systematic schemes in which the transport of the PDF of SGS scalar quantities are

considered. Pope¹⁶ introduced the concept of “filtered density function” (FDF) which is essentially the PDF of SGS scalar variables. With a formal mathematical definition of the FDF, Pope¹⁶ demonstrates that the effects of chemical reaction appear in a closed form in the FDF transport, thus making it a viable candidate for LES of chemically reacting flows. Gao and O’Brien⁴⁶ develop a transport equation for the FDF and offer suggestions for modeling of the unclosed terms in this equation.

The objective of the present work is to further demonstrate the applicability of the FDF and to provide results based on its implementation for LES of chemically reacting turbulent flows. Only the FDF of scalar quantities is considered; probability treatment of the subgrid velocity fluctuations is postponed for future work.

II. FORMULATION

We consider an incompressible (unit density), isothermal, turbulent reacting flow involving N_s species. For the mathematical description of this flow, the primary transport variables are the velocity vector $u_i(\mathbf{x}, t)$ ($i=1,2,3$), the pressure $p(\mathbf{x}, t)$, and the species’ mass fractions $\phi_\alpha(\mathbf{x}, t)$ ($\alpha=1,2,\dots,N_s$). The equations which govern the transport of these variables in space (x_i) and time (t) are

$$\frac{\partial u_i}{\partial x_i} = 0, \quad (1)$$

$$\frac{\partial u_j}{\partial t} + \frac{\partial u_i u_j}{\partial x_i} = -\frac{\partial p}{\partial x_j} + \frac{\partial \tau_{ij}}{\partial x_i}, \quad (2)$$

$$\frac{\partial \phi_\alpha}{\partial t} + \frac{\partial u_i \phi_\alpha}{\partial x_i} = -\frac{\partial J_i^\alpha}{\partial x_i} + \omega_\alpha, \quad (3)$$

where $\omega_\alpha(\mathbf{x}, t) \equiv \hat{\omega}_\alpha(\Phi(\mathbf{x}, t))$ denotes the chemical reaction term for species α , and $\Phi \equiv [\phi_1, \phi_2, \dots, \phi_{N_s}]$ denotes the scalar array. Assuming a Newtonian flow with Fick’s law of diffusion, the viscous stress tensor τ_{ij} and mass flux J_i^α are represented by

$$\tau_{ij} = \nu \left(\frac{\partial u_i}{\partial x_j} + \frac{\partial u_j}{\partial x_i} \right), \quad J_i^\alpha = -\Gamma \frac{\partial \phi_\alpha}{\partial x_i}, \quad (4)$$

where ν is the fluid viscosity and Γ is the diffusion coefficient, $\Gamma = \nu/Sc$, and Sc is the molecular Schmidt number.

Large eddy simulation involves the use of the spatial filtering operation⁴⁷

$$\langle f(\mathbf{x}, t) \rangle_L = \int_{-\infty}^{+\infty} f(\mathbf{x}', t) \mathcal{S}(\mathbf{x}', \mathbf{x}) d\mathbf{x}', \quad (5)$$

where \mathcal{S} denotes the filter function, $\langle f(\mathbf{x}, t) \rangle_L$ represents the filtered value of the transport variable $f(\mathbf{x}, t)$, and $f' = f - \langle f \rangle_L$ denotes the fluctuations of f from the filtered value. We consider spatially and temporally invariant and localized filter functions, thus $\mathcal{S}(\mathbf{x}', \mathbf{x}) \equiv G(\mathbf{x}' - \mathbf{x})$ with the properties,⁴⁷ $G(\mathbf{x}) = G(-\mathbf{x})$, and $\int_{-\infty}^{+\infty} G(\mathbf{x}) d\mathbf{x} = 1$. Moreover, we only consider “positive” filter functions as defined by Verman *et al.*⁴⁸ for which all the moments $\int_{-\infty}^{+\infty} x^m G(x) dx$ exist for $m \geq 0$. The application of the filtering operation to the transport equations yields

$$\frac{\partial \langle u_i \rangle_L}{\partial x_i} = 0, \quad (6)$$

$$\frac{\partial \langle u_j \rangle_L}{\partial t} + \frac{\partial \langle u_i \rangle_L \langle u_j \rangle_L}{\partial x_i} = -\frac{\partial \langle p \rangle_L}{\partial x_j} + \frac{\partial \langle \tau_{ij} \rangle_L}{\partial x_i} - \frac{\partial T_{ij}}{\partial x_i}, \quad (7)$$

$$\frac{\partial \langle \phi_\alpha \rangle_L}{\partial t} + \frac{\partial \langle u_i \rangle_L \langle \phi_\alpha \rangle_L}{\partial x_i} = -\frac{\partial \langle J_i^\alpha \rangle_L}{\partial x_i} - \frac{\partial M_i^\alpha}{\partial x_i} + \langle \omega_\alpha \rangle_L, \quad (8)$$

where $T_{ij} = \langle u_i u_j \rangle_L - \langle u_i \rangle_L \langle u_j \rangle_L$ and $M_i^\alpha = \langle u_i \phi_\alpha \rangle_L - \langle u_i \rangle_L \langle \phi_\alpha \rangle_L$ denote the subgrid stress and the subgrid mass flux, respectively.

III. CLOSURE STRATEGY

In LES of non-reacting flows the closure problem is associated with³ $T_{ij} = \langle u_i u_j \rangle_L - \langle u_i \rangle_L \langle u_j \rangle_L$ and $M_i^\alpha = \langle u_i \phi_\alpha \rangle_L - \langle u_i \rangle_L \langle \phi_\alpha \rangle_L$. In reacting flows, an additional model is required for $\langle \omega_\alpha \rangle_L$. Here, modeling of $\langle \omega_\alpha \rangle_L$ is the subject of the probability formulation as described in the next section. For the former two, we make use of currently available closures which are well-established in non-reacting flows. The subgrid stress is modeled via

$$T_{ij} - (\delta_{ij}/3)T_{kk} = -2\nu_t \langle S_{ij} \rangle_L, \quad (9)$$

where $\langle S_{ij} \rangle_L$ is the resolved strain rate tensor and ν_t is the subgrid viscosity. We use two closures to represent this viscosity. The first is the same as that in the conventional Smagorinsky closure³

$$\nu_t = C_s \Delta_G^2 \sqrt{\langle S_{ij} \rangle_L \langle S_{ij} \rangle_L}, \quad (10)$$

where Δ_G is the filter size and C_s is an empirical constant. The drawbacks of this closure are well-recognized.^{49,50} In an attempt to overcome some of these drawbacks, we also make use of a second closure in which the subgrid viscosity is determined based on the modified subgrid kinetic energy

$$\nu_t = C_k \Delta_G \sqrt{|\langle u_i^* \rangle_L \langle u_i^* \rangle_L - \langle \langle u_i^* \rangle_L \rangle_L \langle \langle u_i^* \rangle_L \rangle_L|}, \quad (11)$$

where $u_i^* = u_i - \mathcal{U}_i$ and \mathcal{U}_i is a reference velocity in the x_i direction. The subscript L' denotes the filter at the secondary level which has a characteristic size (denoted by $\Delta_{G'}$) larger than that of grid level filter. This model is essentially a modified version of that proposed by Bardina *et al.*,⁵¹ which utilize equal sizes for the grid and secondary filters. We refer to this as the modified kinetic energy viscosity (MKEV) closure.

A similar model is used for the closure of the subgrid mass fluxes⁵²

$$M_i^\alpha = -\Gamma_t \frac{\partial \langle \phi_\alpha \rangle_L}{\partial x_i}, \quad (12)$$

where $\Gamma_t = \nu_t/Sc_t$, and Sc_t is the subgrid Schmidt number and is assumed constant.

IV. FILTERED DENSITY FUNCTION (FDF)

The key point in this formulation is to consider the scalar fluctuations of the underlying scalars' array $\Phi(\mathbf{x}, t)$ in a probabilistic manner. For that, we define the "filtered density function" (FDF), denoted by P_L , as¹⁶

$$P_L(\Psi; \mathbf{x}, t) \equiv \int_{-\infty}^{+\infty} \varrho[\Psi, \Phi(\mathbf{x}', t)] G(\mathbf{x}' - \mathbf{x}) d\mathbf{x}', \quad (13)$$

$$\varrho[\Psi, \Phi(\mathbf{x}, t)] = \delta[\Psi - \Phi(\mathbf{x}, t)] \equiv \prod_{\alpha=1}^{N_s} \delta[\psi_\alpha - \phi_\alpha(\mathbf{x}, t)], \quad (14)$$

where δ denotes the delta function and Ψ denotes the composition domain of the scalar array. The term $\varrho[\Phi - \Psi(\mathbf{x}, t)]$ is the "fine-grained" density,^{39,40} and Eq. (13) implies that the FDF is the *spatially filtered* value of the fine-grained density. Thus, P_L gives the density in the composition space of the fluid around \mathbf{x} weighted by the filter G . With the condition of a positive filter kernel,⁴⁸ P_L has all the properties of the PDF.⁴⁰

For further developments, it is useful to define the "conditional filtered value" of the variable $Q(\mathbf{x}, t)$ by

$$\langle Q(\mathbf{x}, t) | \Psi \rangle_L \equiv \frac{\int_{-\infty}^{+\infty} Q(\mathbf{x}', t) \varrho[\Psi, \Phi(\mathbf{x}', t)] G(\mathbf{x}' - \mathbf{x}) d\mathbf{x}'}{P_L(\Psi; \mathbf{x}, t)}, \quad (15)$$

where $\langle \alpha | \beta \rangle_L$ denotes the filtered value of α conditioned on β . Equation (15) implies

$$(i) \text{ For } Q(\mathbf{x}, t) = c, \quad \langle Q(\mathbf{x}, t) | \Psi \rangle_L = c, \quad (16)$$

$$(ii) \text{ For } Q(\mathbf{x}, t) \equiv \hat{Q}(\Phi(\mathbf{x}, t)), \quad \langle Q(\mathbf{x}, t) | \Psi \rangle_L = \hat{Q}(\Psi), \quad (17)$$

(iii) Integral property: $\langle Q(\mathbf{x}, t) \rangle_L$

$$= \int_{-\infty}^{+\infty} \langle Q(\mathbf{x}, t) | \Psi \rangle_L P_L(\Psi; \mathbf{x}, t) d\Psi, \quad (18)$$

where c is a constant, and $\hat{Q}(\Phi(\mathbf{x}, t)) \equiv Q(\mathbf{x}, t)$ denotes the case where the variable Q can be completely described by the compositional variable $\Phi(\mathbf{x}, t)$. From these properties it follows that the filtered value of any function of the scalar variables (such as the reaction rate) is obtained by integration over the composition space

$$\langle Q(\mathbf{x}, t) \rangle_L = \int_{-\infty}^{+\infty} \hat{Q}(\Psi) P_L(\Psi; \mathbf{x}, t) d\Psi. \quad (19)$$

To develop a transport equation for the FDF, the time-derivative of Eq. (13) is considered

$$\begin{aligned} \frac{\partial P_L(\Psi; \mathbf{x}, t)}{\partial t} &= - \int_{-\infty}^{\infty} \frac{\partial \phi_\alpha(\mathbf{x}', t)}{\partial t} \frac{\partial \varrho[\Psi, \Phi(\mathbf{x}', t)]}{\partial \psi_\alpha} \\ &\quad \times G(\mathbf{x}' - \mathbf{x}) d\mathbf{x}' \\ &= - \frac{\partial}{\partial \psi_\alpha} \int_{-\infty}^{\infty} \frac{\partial \phi_\alpha(\mathbf{x}', t)}{\partial t} \\ &\quad \times \varrho[\Psi, \Phi(\mathbf{x}', t)] G(\mathbf{x}' - \mathbf{x}) d\mathbf{x}', \end{aligned} \quad (20)$$

where the summation convention applies to the species suffix, α . This combined with Eq. (15) yields

$$\frac{\partial P_L(\Psi; \mathbf{x}, t)}{\partial t} = - \frac{\partial}{\partial \psi_\alpha} \left[\left\langle \frac{\partial \phi_\alpha}{\partial t} \middle| \Psi \right\rangle_L P_L(\Psi; \mathbf{x}, t) \right]. \quad (21)$$

Substituting Eq. (3) into Eq. (21) yields

$$\begin{aligned} \frac{\partial P_L(\Psi; \mathbf{x}, t)}{\partial t} &= \frac{\partial}{\partial \psi_\alpha} \left\{ \left[\left\langle \frac{\partial u_i \phi_\alpha}{\partial x_i} \middle| \Psi \right\rangle_L + \left\langle \frac{\partial J_i^\alpha}{\partial x_i} \middle| \Psi \right\rangle_L \right. \right. \\ &\quad \left. \left. - \langle \hat{\omega}_\alpha(\Phi) | \Psi \rangle_L \right] P_L(\Psi; \mathbf{x}, t) \right\} \end{aligned} \quad (22)$$

in which the convective term can be represented in the form

$$\begin{aligned} \frac{\partial}{\partial \psi_\alpha} \left[\left\langle \frac{\partial u_i \phi_\alpha}{\partial x_i} \middle| \Psi \right\rangle_L P_L(\Psi; \mathbf{x}, t) \right] \\ = - \frac{\partial \langle u_i | \Psi \rangle_L P_L(\Psi; \mathbf{x}, t)}{\partial x_i}. \end{aligned} \quad (23)$$

The unclosed nature of convection is denoted by the conditional filtered value of the velocity which is further decomposed into resolved and subgrid scale components. It is useful to adopt the decomposition

$$\langle u_i | \Psi \rangle_L P_L = \langle u_i \rangle_L P_L + [\langle u_i | \Psi \rangle_L - \langle u_i \rangle_L] P_L, \quad (24)$$

so that Eq. (21) can be expressed as

$$\begin{aligned} \frac{\partial P_L}{\partial t} + \frac{\partial \langle u_i \rangle_L P_L}{\partial x_i} &= - \frac{\partial [\langle u_i | \Psi \rangle_L - \langle u_i \rangle_L] P_L}{\partial x_i} \\ &\quad + \frac{\partial}{\partial \psi_\alpha} \left[\left\langle \frac{\partial J_i^\alpha}{\partial x_i} \middle| \Psi \right\rangle_L P_L \right] \\ &\quad - \frac{\partial [\hat{\omega}_\alpha(\Psi) P_L]}{\partial \psi_\alpha}. \end{aligned} \quad (25)$$

This is an exact transport equation for the FDF and is similar to that presented by Gao and O'Brien.⁴⁶ The last term on the right hand side of this equation is due to chemical reaction and is in a closed form. The second term on the left hand side represents the filtered convection of the FDF in physical space and is also closed (provided $\langle u_i \rangle_L$ is known). The unclosed terms are associated with the first term on the right hand side denoting the effects of unresolved subgrid scale convection, and the second term on the right hand side representing the influence of molecular diffusion.

The subgrid convective flux is modeled via

$$[\langle u_i | \Psi \rangle_L - \langle u_i \rangle_L] P_L = - \Gamma_\tau \frac{\partial P_L}{\partial x_i}. \quad (26)$$

The advantage of the decomposition (Eq. (24)) and the subsequent model (Eq. (26)) is that they yield results similar to that in conventional LES for the first moment of the FDF. The first moments corresponding to Eqs. (24) and (26) are

$$\langle u_i \phi_\alpha \rangle_L = \langle u_i \rangle_L \langle \phi_\alpha \rangle_L + [\langle u_i \phi_\alpha \rangle_L - \langle u_i \rangle_L \langle \phi_\alpha \rangle_L], \quad (27)$$

$$[\langle u_i \phi_\alpha \rangle_L - \langle u_i \rangle_L \langle \phi_\alpha \rangle_L] = - \Gamma_\tau \frac{\partial \langle \phi_\alpha \rangle_L}{\partial x_i}, \quad (28)$$

respectively. The term in brackets in Eq. (27) is the generalized scalar flux in the form considered in conventional LES (Ref. 14) as pointed out by Gao and O'Brien.⁴⁶ Consequently, Eq. (28) becomes identical to Eq. (12).

The closure for the conditional subgrid diffusion is based on the linear mean square estimation (LMSE) (Refs. 39, 53) model, which is also known as the IEM (Ref. 54) (interaction by exchange with the mean) closure. The model involves the decomposition of the diffusion term in Eq. (25),

$$\begin{aligned} \frac{\partial}{\partial \psi_\alpha} \left[\left\langle -\frac{\partial}{\partial x_i} \left(\Gamma \frac{\partial \phi_\alpha}{\partial x_i} \right) \middle| \Psi \right\rangle_L P_L \right] \\ = \frac{\partial}{\partial x_i} \left(\Gamma \frac{\partial P_L}{\partial x_i} \right) - \frac{\partial^2}{\partial \psi_\alpha \partial \psi_\beta} \left[\left\langle \Gamma \frac{\partial \phi_\alpha}{\partial x_i} \frac{\partial \phi_\beta}{\partial x_i} \middle| \Psi \right\rangle_L P_L \right]. \end{aligned} \quad (29)$$

The first term on the right hand side of this equation denotes the effects of molecular diffusion in spatial transport of the FDF. The second term represents the dissipative nature of subgrid scalar mixing. The LMSE model suggests

$$\begin{aligned} \frac{\partial^2}{\partial \psi_\alpha \partial \psi_\beta} \left[\left\langle \Gamma \frac{\partial \phi_\alpha}{\partial x_i} \frac{\partial \phi_\beta}{\partial x_i} \middle| \Psi \right\rangle_L P_L \right] \\ = -\frac{\partial}{\partial \psi_\alpha} [\Omega_m (\psi_\alpha - \langle \phi_\alpha \rangle_L) P_L], \end{aligned} \quad (30)$$

where Ω_m is the ‘‘frequency of mixing within the subgrid’’ which is not known *a priori*. Analogous to the procedures in Reynolds averaged methods, this frequency can be related to the subgrid diffusion coefficient and the filter length: $\Omega_m = C_\Omega (\Gamma + \Gamma_t) / \Delta_G^2$. The second moment of Eq. (30) provides an expression for the total subgrid scalar dissipation

$$\epsilon_\alpha = 2\Gamma \left\langle \frac{\partial \phi_\alpha}{\partial x_i} \frac{\partial \phi_\alpha}{\partial x_i} \right\rangle_L = 2\Omega_m (\langle \phi_\alpha^2 \rangle_L - \langle \phi_\alpha \rangle_L^2), \quad (31)$$

where subscripts in parentheses are excluded from the summation convention. With the closures given by Eqs. (26) and (30), the modeled FDF transport equation is

$$\begin{aligned} \frac{\partial P_L}{\partial t} + \frac{\partial [\langle u_i \rangle_L P_L]}{\partial x_i} = \frac{\partial}{\partial x_i} \left[(\Gamma + \Gamma_t) \frac{\partial P_L}{\partial x_i} \right] \\ + \frac{\partial}{\partial \psi_\alpha} [\Omega_m (\psi_\alpha - \langle \phi_\alpha \rangle_L) P_L] \\ - \frac{\partial [\hat{\omega}_\alpha(\Psi) P_L]}{\partial \psi_\alpha}. \end{aligned} \quad (32)$$

This equation may be integrated to obtain transport equations for the SGS moments. The equation for the first subgrid moment, $\langle \phi_\alpha \rangle_L$, and the generalized subgrid variance, $\sigma_\alpha = \langle \phi_\alpha^2 \rangle_L - \langle \phi_\alpha \rangle_L^2$ are

$$\frac{\partial \langle \phi_\alpha \rangle_L}{\partial t} + \frac{\partial \langle u_i \rangle_L \langle \phi_\alpha \rangle_L}{\partial x_i} = \frac{\partial}{\partial x_i} (\Gamma + \Gamma_t) \frac{\partial \langle \phi_\alpha \rangle_L}{\partial x_i} + \langle \omega_\alpha \rangle_L, \quad (33)$$

$$\begin{aligned} \frac{\partial \sigma_\alpha}{\partial t} + \frac{\partial \langle u_i \rangle_L \sigma_\alpha}{\partial x_i} = \frac{\partial}{\partial x_i} \left[(\Gamma + \Gamma_t) \frac{\partial \sigma_\alpha}{\partial x_i} \right] - 2\Omega_m \sigma_\alpha \\ + 2(\Gamma + \Gamma_t) \left[\frac{\partial \langle \phi_\alpha \rangle_L}{\partial x_i} \frac{\partial \langle \phi_\alpha \rangle_L}{\partial x_i} \right] \\ + 2(\langle \phi_\alpha \omega_\alpha \rangle_L - \langle \phi_\alpha \rangle_L \langle \omega_\alpha \rangle_L). \end{aligned} \quad (34)$$

These equations are identical to those which can be derived by filtering Eq. (3) directly, and adopting Eqs. (12) and (31) for the subgrid flux and dissipation. In such direct moment closure formulation, however, the terms involving $\langle \omega_\alpha \rangle_L$ remain unclosed. It is observed that the modeled FDF equation (Eq. (32)) is similar in form to the standard modeled equation for the joint PDF of composition.⁴⁰

V. MONTE CARLO SOLUTION OF THE FDF

The solution of the FDF transport equation (Eq. (32)) provides all the statistical information pertaining to the scalar variable $\Phi(\mathbf{x}, t)$. This equation can be solved most effectively via the Monte Carlo scheme. In PDF methods the Monte Carlo schemes can be utilized in both Eulerian⁵⁵ and Lagrangian^{40,56} contexts. Thus, it is expected that both of the procedures can be potentially employed for the solution of the FDF. In the Eulerian Monte Carlo scheme, the FDF is represented by an ensemble of computational elements (or particles) at ‘‘fixed’’ grid points. These elements are transported in the ‘‘physical space’’ by the combined actions of resolved scale convection and diffusion (molecular and subgrid). In addition, transport in the composition space occurs due to chemical reaction and subgrid mixing. Prior to this work, the Eulerian Monte Carlo method was implemented. Expectedly, the results were not encouraging. The major difficulty with the Eulerian formulation lies in the numerical implementation of the resolved scale convection. The numerical implementation via a first order accurate upwind scheme was shown to produce excessive artificial diffusion errors. While such errors can be tolerated in PDF methods (at least for some flows), they degrade the LES results. In some cases the numerical errors become significantly larger than the subgrid and molecular diffusions.

A remedy for the problem noted above is to divorce from the Eulerian discretization and to invoke the Monte Carlo solver in a ‘‘grid free’’ Lagrangian manner. The advantages of Lagrangian numerical methods in reducing the amount of numerical diffusion are well-recognized.⁵⁷⁻⁶² The basis of the Lagrangian solution of the FDF transport equation relies upon the principle of *equivalent systems*.^{40,56} Two systems with different instantaneous behaviors may have identical statistics and satisfy the same FDF transport equation. In the Lagrangian Monte Carlo procedure each of the particles obeys certain equations which govern its transport. These particles undergo motion in the physical space by convection due to the filtered mean flow velocity, and diffusion due to molecular and subgrid diffusivities. The general diffusion process is represented in a stochastic manner by the following stochastic differential equation (SDE) (Refs. 40, 63, 64),

$$dX_i(t) = D_i(\mathbf{X}(t), t)dt + E(\mathbf{X}(t), t)dW_i(t), \quad (35)$$

where X_i is the Lagrangian position of a stochastic particle, D_i and E are known as the ‘‘drift’’ and ‘‘diffusion’’ coefficients, respectively, and W_i denotes the Wiener-Lévy process.⁶⁵ A comparison of the Fokker-Plank equation corresponding to Eq. (35) with the FDF transport equation (32) determines the appropriate specification of the coefficients to be

$$E \equiv \sqrt{2(\Gamma + \Gamma_t)}, \quad D_i \equiv \langle u_i \rangle_L + \frac{\partial(\Gamma + \Gamma_t)}{\partial x_i}. \quad (36)$$

Thus the SDE which represents the spatial transport of the FDF is

$$dX_i(t) = \left[\langle u_i \rangle_L + \frac{\partial(\Gamma + \Gamma_t)}{\partial x_i} \right] dt + [2(\Gamma + \Gamma_t)]^{1/2} dW_i. \quad (37)$$

The compositional makeup of the particles evolves simultaneously due to the actions of subgrid mixing and reaction

$$\frac{d\phi_\alpha^+}{dt} = -\Omega_m(\phi_\alpha^+ - \langle \phi_\alpha \rangle_L) + \omega_\alpha, \quad (38)$$

where $\phi_\alpha^+ = \phi_\alpha(X_i(t), t)$ denotes the scalar value of the particle with the Lagrangian position vector X_i .

In the numerical implementation, the FDF is represented by an ensemble of Monte Carlo particles, each with a set of scalars $\phi_\alpha^{(n)}(\mathbf{X}^{(n)}(t), t)$ and Lagrangian position vector $\mathbf{X}^{(n)}$. Numerically, a splitting operation is employed in which the transport in the physical and the compositional domains are treated separately. The simplest means of simulating Eq. (37) is via the Euler-Maruyama approximation⁶⁶

$$X_i^n(t_{k+1}) = X_i^n(t_k) + D_i^n(t_k)\Delta t + E^n(t_k)(\Delta t)^{1/2}\xi_i^n(t_k), \quad (39)$$

where $D_i^n(t_k) = D_i(\mathbf{X}^{(n)}(t_k), t)$, $E^n(t_k) = E(\mathbf{X}^{(n)}(t_k), t)$ and $\xi_i^{(n)}$ is a random variable with the standard Gaussian PDF. This formulation preserves the Markovian character of the diffusion process⁶⁷⁻⁶⁹ and facilitates affordable computations. Higher order numerical schemes for solving Eq. (37) are available,⁶⁶ but one must be cautious in using them for LES since the diffusion term in Eq. (35) depends on the stochastic process $\mathbf{X}(t)$. The numerical scheme must preserve the Itô-Gikhman^{70,71} nature of the process. The coefficients D_i and E require the input of the filtered mean velocity and the diffusivity (molecular and subgrid eddy). These are provided by the solution of Eqs. (6)–(12) by a finite difference LES (as described below) on a fixed grid and then interpolated to the particle location.

The compositional values are subject to change due to subgrid mixing and chemical reaction. Equation (38) may be integrated numerically to simulate these effects simultaneously. Alternately, this equation is treated in a split manner. This provides an analytical expression for the subgrid mixing. Subsequently, the influence of chemical reaction is determined by evaluating the fine grained reaction rates ω_α^n and modifying the composition of the elements. The implementation of the SGS mixing and chemical reaction requires the filtered mean values of the scalars. These mean values

(and other higher moments of the FDF) at a given point are estimated by consideration of particles within some volume centered at the point of interest. Effectively, this finite volume constitutes an ‘‘ensemble domain’’ characterized by the length scale Δ_E (not to be confused with Δ_G) in which the FDF is represented discretely by stochastic particles. This is necessary as, with probability one, no particles will coincide with the point as considered.⁵⁶ Here, a box of size Δ_E is used to construct the ensemble mean values at the finite difference nodes. These values are then interpolated to the particle positions. Since the mixing model only requires the input of the filtered scalar value, and not its derivative, this volume averaging procedure is sufficient. However, from the numerical standpoint, determination of the size of the ensemble domain is an important issue. Ideally, it is desired to obtain the statistics from the Monte Carlo solution when the size of sample domain is infinitely small (i.e., $\Delta_E \rightarrow 0$) and the number of particles within this domain is infinitely large. With a finite number of particles, if Δ_E is small there may not be enough particles to construct the statistics. A larger ensemble domain decreases the statistical error, but may increase the dispersion error which manifests itself in ‘‘artificially diffused’’ statistical results. This compromise between the statistical accuracy and dispersive accuracy as pertaining to Lagrangian Monte Carlo schemes implies that the optimum magnitude of Δ_E cannot, in general, be specified *a priori*.⁴⁰ This does not diminish the capability of the procedure, but exemplifies the importance of the parameters which govern the statistics.

The LES of the hydrodynamic variables, which also determines the subgrid viscosity and scalar diffusion coefficients, is conducted with the ‘‘compact parameter’’ finite difference scheme of Carpenter.⁷² This is a variant of the McCormack⁷³ scheme in which a fourth order compact differences are used to approximate the spatial derivatives, and a second order symmetric predictor-corrector sequence is employed for time discretization. The computational scheme is based on a hyperbolic solver which considers a fully compressible flow. Here, the simulations are conducted with a low Mach number ($M \approx 0.3$) to minimize compressibility effects. The procedure involved in the finite difference discretization is independent of the Monte Carlo solver, thus alternative differencing schemes can be used if desired. All the finite difference operations are conducted on fixed and equally sized grid points. The transfer of information from these points to the locations of the Monte Carlo particles is conducted via interpolation. Both fourth-order and second-order (bilinear) interpolation schemes were considered, but no significant differences in SGS statistics were observed. The results presented in the next section are based on simulations with fourth- and second-order interpolations in two-dimensional (2D) and 3D flows, respectively.

VI. RESULTS

A. Flows simulated

To demonstrate the effectiveness of the FDF method, in this section simulation results are presented of a temporally developing mixing layer and a spatially developing planar

jet. Both non-reacting and reacting flows are considered. In the latter, a simple reaction of the type $\mathcal{A} + \mathcal{B} \rightarrow \mathcal{P}$ is considered in which the reaction is assumed to be constant rate and non-heat releasing (isothermal flow). Therefore, $\omega_{\mathcal{A}} = \omega_{\mathcal{B}} = -KAB$, where K is a constant and A, B denote the mass fractions of species \mathcal{A}, \mathcal{B} , respectively. The species $\mathcal{A}, \mathcal{B}, \mathcal{P}$ are assumed thermodynamically identical and the fluid is assumed to be calorically perfect. Both 2D and 3D simulations are conducted of the temporal mixing layer. The jet simulations are 2D.

The temporal mixing layer consists of two coflowing streams traveling in opposite directions with the same speed.^{74–77} The reactants \mathcal{A} and \mathcal{B} are introduced into the top and the bottom streams, respectively. In the planar jet, the reactant \mathcal{A} is injected with a high velocity from a jet of width D into a coflowing stream with a lower velocity carrying reactant \mathcal{B} .^{76,78} Both these flows are dominated by large scale coherent structures. The formation of these structures are expedited by imposing low amplitude perturbations. In the figures presented below, x, y correspond to the streamwise and cross-stream directions, respectively. In 3D, z denotes the spanwise direction. In the temporal mixing layer, the length in the streamwise direction is chosen to be twice the wavelength of the most unstable mode to allow for the rollup of two large vortices and one (subsequent) pairing of these vortices. In 3D, the lengths in the streamwise and the cross-stream directions are the same as those in 2D. The length in the spanwise direction is 60% of that in the streamwise direction. The forcing is imposed in such a way to provide significant 3D transport.^{79,80} The initial values of the mass fractions of reactants \mathcal{A} and \mathcal{B} at each of the spanwise points in 3D are identical to those in 2D. The size of the domain in the jet flow is $0 \leq x \leq 14D$, $-3.5D \leq y \leq 3.5D$. The velocity ratio of the coflowing stream to that of the inlet jet is kept fixed at 0.5.

Both flows are simulated via both DNS and LES. The procedure in DNS is exclusively based on the finite-difference solution of Eqs. (1)–(4) in which there are sufficient grid points to resolve the flow without a need for subgrid closures. The procedure in LES is based on the Monte Carlo solution of the modeled FDF transport equation (Eq. (32)) for the scalars augmented by the finite difference solution of the modeled equations of the filtered hydrodynamic variables (Eqs. (6)–(7)). In the presentation below, these results are identified by the abbreviation FDF. In addition, another LES is conducted in which the modeled transport equations for the filtered scalar and the generalized subgrid variance are simulated with the finite difference scheme. In these simulations, the hydrodynamic solver and the models for the subgrid stresses and mass fluxes are identical to those employed in FDF, but the effects of SGS fluctuations in the filtered reaction rate are ignored. Effectively, Eqs. (33)–(34) are solved with the assumption $\langle \omega_{\alpha}(\Phi) \rangle_L = \omega_{\alpha}(\langle \Phi \rangle_L)$. The results based on this procedure are referred to as LES-FD. (The approximation $\langle \omega_{\alpha}(\Phi) \rangle_L = \langle \omega_{\alpha}(\langle \Phi \rangle_L) \rangle_L$ was also considered but did not show an improvement over LES-FD.)

In both FDF and LES-FD simulations, the subgrid stresses are modeled via the Smagorinsky closure (Eqs. (9)–(10)) and the MKEV model (Eq. (11)). The subgrid mass

fluxes are modeled via Eq. (12). No attempt is made here to determine the magnitudes of the constants appearing in these models in a dynamic manner.¹⁴ However, several different values are considered for C_s and C_k . The values which give the best overall agreement with DNS in non-reacting flows are $C_s = 0.014, 0.01$ and $C_k = 0.02, 0.013$, in 2D, 3D, respectively. These values are subsequently used in FDF and LES-FD of scalar quantities in reacting flows. This parameterization is justified since the LES of the hydrodynamic field is not the subject of our FDF closure. The other parameters $Sc = 1, Sc_t = 0.7$ are kept fixed. In the MKEV model, the ratio of the filter size at the secondary level to that at the grid level is $\Delta_{G'} / \Delta_G = 3$. In the implementation of the MKEV in the shear flows as considered, the magnitude of the reference velocity \mathcal{U}_i is set to zero in the cross-stream direction and to the average of the high and low speed streams in the streamwise direction. The subgrid mixing model requires the input of the constant C_{Ω} in the mixing frequency which also determines the SGS variances. As will be shown below $C_{\Omega} \approx 3$ is suggested, but the influence of this parameter is also studied by considering other C_{Ω} values.

The flow variables are normalized with respect to reference quantities denoted by the subscript r . In the temporal mixing layer the reference quantities are the freestream values and the length L_r is defined such that $(\delta_{v0} / L_r) = 2.83$, where δ_{v0} is the initial vorticity thickness. In the planar jet, $L_r = D$ and the reference quantities are those at the high speed jet stream. The reference quantities define the Reynolds number $Re = (U_r L_r / \nu)$. For the temporal mixing layer, the Reynolds number based on the total velocity difference across the layer ($\Delta U = 2U_r$) is given by $Re_{\delta_{v0}} = 5.66 Re$. The reaction rate is parameterized by the Damköhler number $Da = K / (U_r / L_r)$. The non-dimensional time is given by $t^* = (U_r t / L_r)$. In the presentations below, the asterisk is dropped.

B. Numerical specifications

The magnitude of the flow parameters considered in the simulations are dictated by the resolution which can be afforded by DNS. The primary parameters are the flow Reynolds number (Re), the Damköhler number (Da) and the molecular Schmidt number. All finite difference simulations (in both DNS and LES) are conducted on equally-spaced, square ($\Delta x = \Delta y = \Delta z$ (for 3D) = Δ) grids. Since the size of the computational domain is fixed, the number (and the size) of the grids depends on type of simulation being conducted. The highest resolution in DNS of the 2D temporal mixing layer consists of 433×577 grid points which allows reliable DNS with $Re = 500$ and $Da = 2$ (based on the velocity difference and the vorticity thickness at the initial time). The DNS of the 3D temporal mixing layer is conducted on $217 \times 289 \times 133$ grid points with $Re = 400, Da = 1$. The resolution in DNS of the planar jet consists of 721×361 grid points and allows accurate simulations with $Re = 12\,000$ and $Da = 2$ (based on the centerline velocity at the inlet and the jet width).

The FDF and LES-FD are conducted on grids coarser

than those in DNS. Unless otherwise specified, the LES resolutions in the mixing layer consist of 37×49 grid points in 2D, and $55 \times 73 \times 34$ grid points in 3D. For the planar jet, a resolution of 101×51 is used for nonreacting flow simulations with $Re=5000$, while a 181×91 grid is utilized for reactive flow simulations with $Da=2$ and $Re=12\,000$. A top-hat filter function⁴⁷ of the form below is used

$$G(\mathbf{x}' - \mathbf{x}) = \prod_{i=1}^{N_D} \tilde{G}(x'_i - x_i), \quad (40)$$

$$\tilde{G}(x'_i - x_i) = \begin{cases} \frac{1}{\Delta_G} & |x'_i - x_i| \leq \frac{\Delta_G}{2} \\ 0 & |x'_i - x_i| > \frac{\Delta_G}{2} \end{cases}$$

in which N_D denotes the number of dimensions, and $\Delta_G = 2\Delta$. No attempt is made to investigate the sensitivity of the results to the filter function⁴⁸ or the size of the filter.⁸¹

In FDF, the Monte Carlo particles are distributed at $t = 0$ throughout the domain. In the temporal mixing layer, the particles are distributed evenly throughout the whole computational region. In the FDF of the jet, the particles are supplied initially in the inlet region $-1.75D \leq y \leq 1.75D$. In all the simulations, the particle density is monitored at all times to ensure an approximately uniform distribution throughout the mixing regions. In the temporal mixing layer, due to flow periodicity in the streamwise direction, if the particle leaves the domain at the right or the left boundary, new particles are introduced at the other boundary with the same compositional values. A similar procedure is employed in the spanwise direction in 3D simulations. Due to mirror symmetry at the upper and lower boundaries, particles that exit the top or bottom boundaries return to the domain at the opposite boundary with the mass fractions values associated with \mathcal{A} and \mathcal{B} interchanged. In the spatial jet, new particles are introduced at the inlet at a rate proportional to the local flow velocity and with a compositional makeup dependent on the y coordinate. The density of the Monte Carlo particles is determined by the initial number of particles per grid cell (NPG) of dimension $\Delta \times \Delta$ ($\times \Delta$ in 3D). The magnitude of NPG is varied to assess its affect on statistical convergence of the Monte Carlo results. This assessment is demonstrated in 2D simulations of the temporal mixing layer. The simulations of 3D temporal layer and the spatial jet are based on $NPG=20$. The size of the “ensemble domain” in the FDF simulations is also varied to assess its influence on the statistical convergence. The following sizes are considered: $\Delta_E = 2\Delta, \Delta, \Delta/2$. The number of samples used to construct the FDF is thus controlled by the values of NPG and Δ_E .

An additional parameter which influences the numerical accuracy is the magnitude of the incremental time step. The stability criterion for the finite difference scheme requires⁷² $CFL \leq 1/\sqrt{3}$ and is more stringent than the criterion for the Fourier number. The effect of the time increment on the accuracy of the Euler-Maruyama scheme is also considered. This is assessed by considering several Δt values (CFL

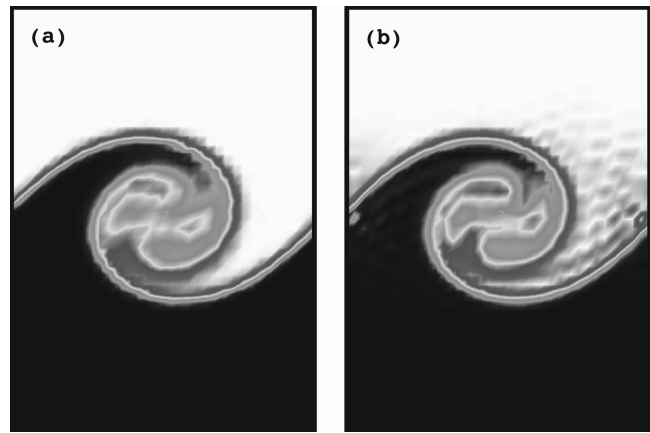


FIG. 1. 2D mixing layer simulation results: Contours of the filtered conserved scalar. (a) FDF and (b) LES-FD.

numbers). In the context of Itô calculus,^{82,83} this issue is considered by analysis of moments of the FDF up to the second order.

The simulated results are analyzed both “instantaneously” and “statistically.” In the former, the instantaneous contours (snap-shots) of the scalar values are considered. In the latter, the “Reynolds-averaged” statistics constructed from the instantaneous data are considered. In the spatially developing jet flow this averaging procedure is conducted via sampling in time. In the temporal mixing layer, the flow is homogeneous in x (and z in 3D); thus the statistics are generated by constructing the ensemble from all the grid points in the streamwise (and spanwise) directions. These statistics are $y-t$ dependent. All Reynolds averaged results are denoted by an overbar.

C. Consistency of FDF and convergence of the Monte Carlo procedure

The objective in the results presented in this subsection is to demonstrate the consistency of the FDF formulation and the convergence of the Monte Carlo simulations. For this purpose, the LES results via FDF and LES-FD are compared against each other in shear flows under different conditions. In non-reacting flows, any deviations between the FDF and LES-FD results are attributed to the differences in the numerical procedures. Since the accuracy of the finite difference procedure is well-established, this comparative analysis provides a good means of assessing the performance of the Monte Carlo solution of the FDF. Unless specified otherwise, the Smagorinsky model is used to evaluate the eddy viscosity in the simulations considered in this subsection.

In Fig. 1, results are presented of the LES of the non-reacting temporally developing mixing layer. Shown in the figure are the contour plots of $\langle A \rangle_L$ via (a) FDF and (b) LES-FD, with $A=0, 1$ on the bottom and top streams, respectively. These contours correspond to results at a time when the flow has experienced the pairing of two neighboring vortices. This figure provides a simple visual demonstration of the consistency of the FDF as the results via the particle method are in agreement with those obtained by LES-FD. In fact, the Monte Carlo results are somewhat more

attractive due the Lagrangian nature of the solution procedure. While the LES-FD results display slight over- and under-shoots, there are no such errors in the Monte Carlo scheme.

A more rigorous means of assessing the FDF results is via consideration of the Reynolds averaged results. Figures 2 and 3 show such results in the non-reacting temporal mixing layer in which the sensitivity of the FDF predictions to several parameters is assessed. Figure 2(a) shows the comparison of FDF and LES-FD results for $\langle A \rangle_L$ for several values of Δ_E . It is shown that the first filtered moment of the FDF agrees very well with that obtained by LES-FD, even for large Δ_E values. The differences between the FDF and LES-FD results are more apparent in Figs. 2(b,c,d) where the cross-stream variations of σ_A are shown for several values of Δ_E and C_Ω and for different LES grid resolutions. As expected, Figs. 2(b,c) show that with increasing C_Ω , the magnitude of the variance decreases. These figures also indicate that the difference between FDF and LES-FD predictions diminish as Δ_E decreases. This is also corroborated in Fig. 2(d) in which the both FDF and LES-FD are conducted on 61×81 grid points. At all Δ_E values, the agreement between FDF and LES-FD is better than those shown in Fig. 2(b) with a lower finite difference resolution. The consistency of the FDF and LES-FD results does not mean that the magnitude of C_Ω can be specified. Hereinafter $C_\Omega = 3$ is adopted since it provides the best overall match with DNS data as shown in the next subsection.

The other parameters which influence the accuracy of the Monte Carlo results are the number of Monte Carlo particles per grid cell (NPG) and the magnitude of the incremental time step. Figure 3(a) shows that $\overline{\sigma_A}$ values do not vary significantly for $\text{NPG} > 50$. In fact in other cases even smaller NPG values can be used as will be shown. Figure 3(b) verifies the insensitivity of statistics to Δt as long as the stability criterion is satisfied ($\text{CFL} \leq 1/\sqrt{3}$). Hereinafter, $\text{CFL} = 0.5$ is used.

The sensitivity of the results to NPG and Δ_E in the FDF simulations of a reacting temporal mixing layer with $\text{Da} = 2$ is studied in Fig. 4. In these simulations, the MKEV model is adopted to evaluate the subgrid viscosity because it performs somewhat better than the Smagorinsky model for LES of reactive flows (as assessed by DNS data in the next subsection). Shown in the figure are the Reynolds averaged values of the filtered product mass fraction ($\langle P \rangle_L$) at a fixed time (Fig. 4(a)) and the integrated total product ($\delta p(t) = \int \langle P \rangle_L(y, t) dy$). The convergence of Monte Carlo solution and the independence to NPG and Δ_E are demonstrated by these results (at least for this first moment). Moreover, it is shown that while the mean value of the scalar as used in the mixing model for a given particle should be evaluated at the particle location, the mean value at the nearest finite difference grid point could also be substituted. This eliminates the need for interpolating the mean scalar field to the particle locations.

The consistency and the convergence of the Monte Carlo simulation of the FDF in the nonreacting jet flow are summarized in Figs. 5–6 in which the time averaged (Reynolds)

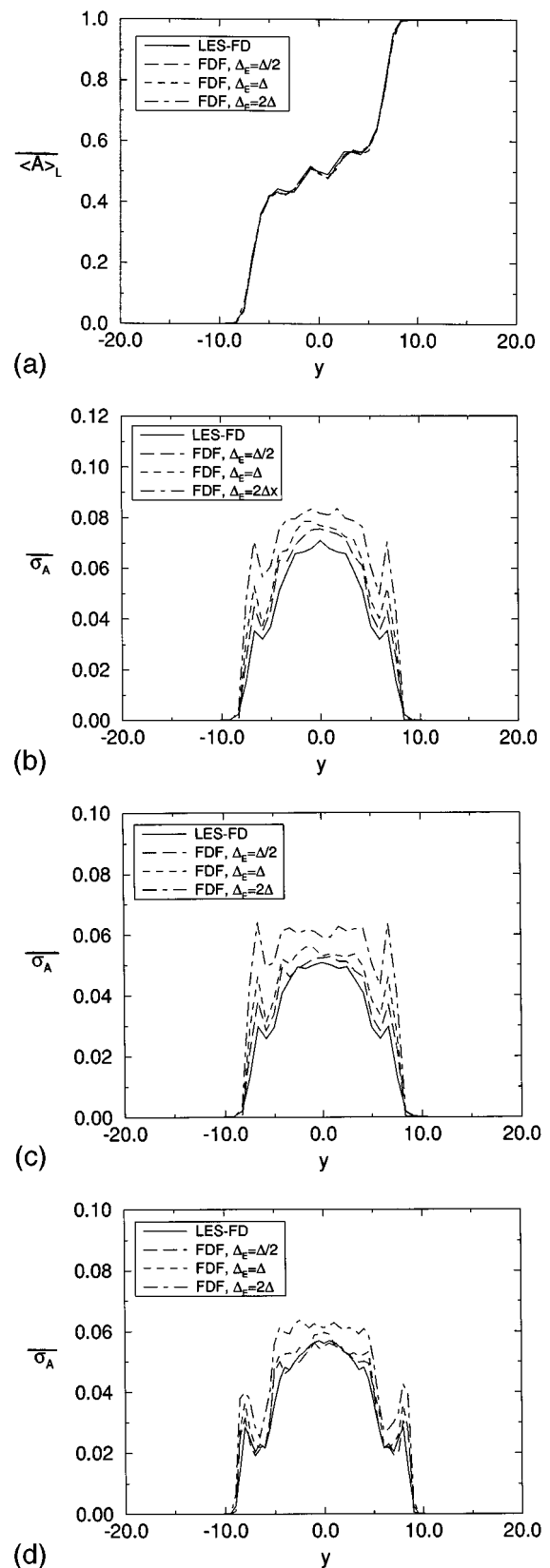


FIG. 2. 2D mixing layer simulation results: (a) Conserved scalar distribution vs. the cross-stream coordinate. Generalized variance vs. cross-stream coordinate at (b) $C_\Omega = 1$ and (c) $C_\Omega = 3$. (d) Same as (b) but with increased resolution.

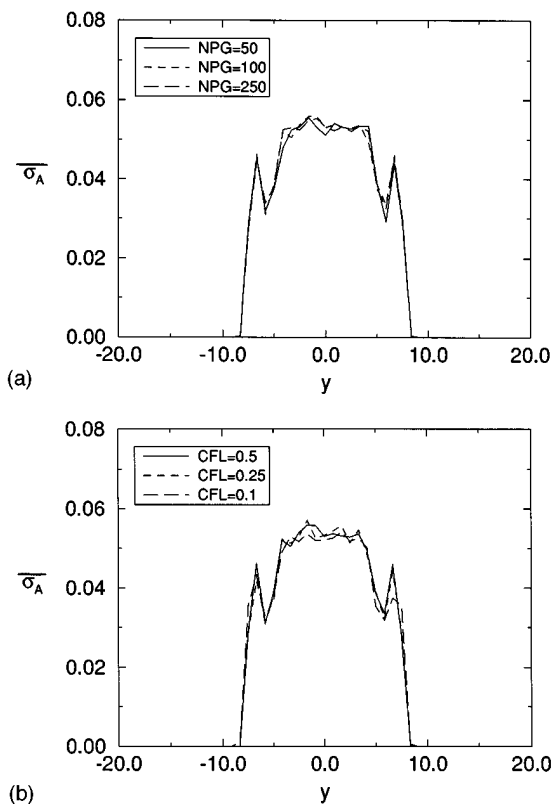


FIG. 3. 2D mixing layer simulation results: (a) Cross-stream variation of the generalized variance for various NPG. (b) Generalized variance vs. cross-stream coordinate at various CFL numbers.

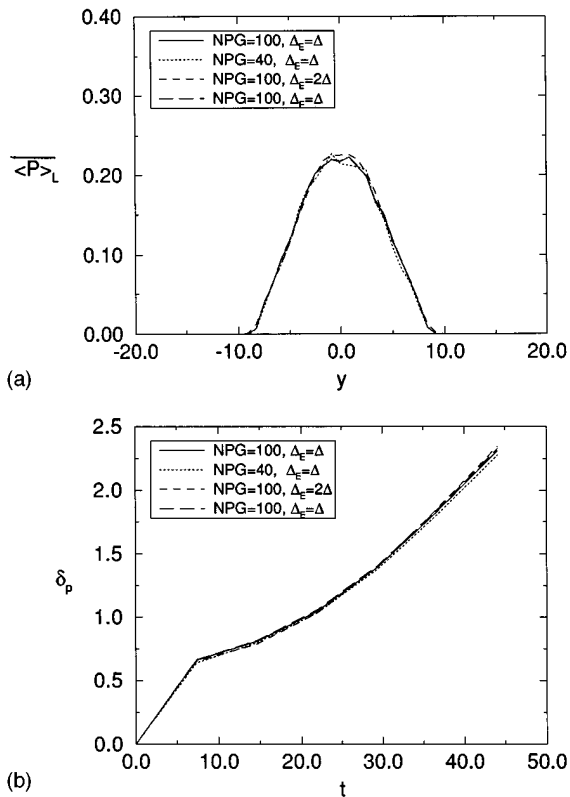


FIG. 4. 2D mixing layer simulation results: (a) Cross-stream variation of the product mass fraction. (b) Total product vs. time. The long-dashed line represent the case where the mean value of the scalar in the mixing model for a particle is set to be equal to the value at the nearest finite difference grid point.

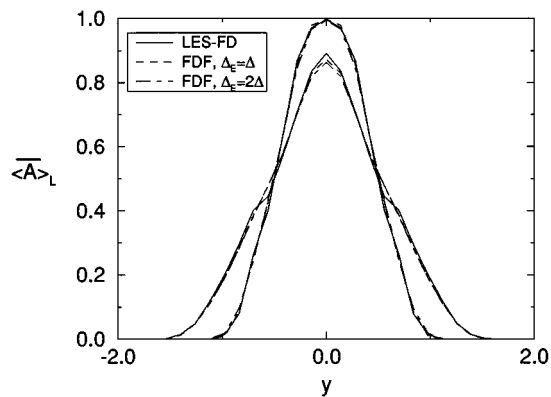


FIG. 5. 2D planar jet results: Conserved scalar distribution vs. cross-stream coordinate at $x=5D, 9D$.

statistics for the first and second subgrid moments of A are presented. Similar to the temporal mixing layer results, Fig. 5 shows the accuracy of the Monte Carlo solver and the insensitivity of results to Δ_E for the first moment of the FDF. Similarly, for the scalar variance, the agreement between the FDF and LES-FD results diminishes as the size of Δ_E is decreased. At $x=5D$, the FDF results with $\Delta_E = \Delta$ are very close to those via LES-FD. With the same Δ_E values the agreement is not as good at $x=9D$ and lower values of Δ_E are needed to achieve a better agreement for the subgrid variance. However, as will be shown below, with this reso-

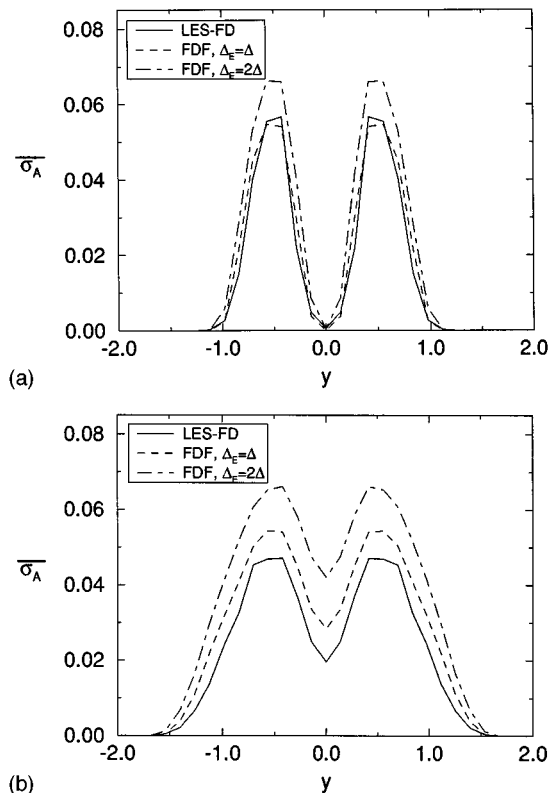


FIG. 6. 2D planar jet results: Generalized variance vs. cross-stream coordinate at (a) $x=5D$ and (b) $x=9D$.

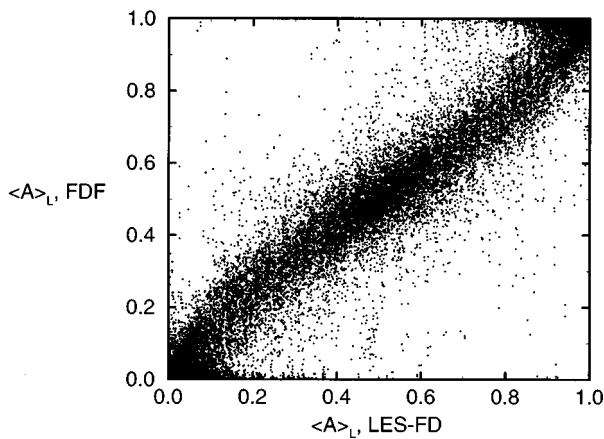


FIG. 7. 3D mixing layer simulation results: Scatter plot of the filtered values of a conserved scalar as obtained by FDF vs. those via LES-FD.

lution the mean filtered values of reacting scalars are predicted reasonably well.

The consistency of the FDF simulation in 3D is demonstrated in Fig. 7 in which the scatter plot is shown of the instantaneous filtered A values as obtained by FDF vs. those via LES-FD. The hydrodynamic LES is based on MKEV in both simulations. The correlation coefficient between the data obtained by the two simulations is 0.99. This excellent correlation is also reflected in the cross stream profiles of the Reynolds-averaged filtered quantities in Fig. 8.

D. DNS validations of the FDF

The objective in this section is to assess the overall performance of the FDF and to appraise the validity of the sub-models employed in the FDF transport equation. For this objective, the FDF results are compared against DNS of the same flow configuration with the same magnitudes of Re and Da . For a meaningful comparison, the DNS data are filtered and the results on the coarse grids are compared with those on the corresponding coarse grids in the FDF simulations. To illustrate the capability of the FDF, the results are also compared with LES-FD in which the effects of SGS fluctuations on the filtered reaction rate are ignored.

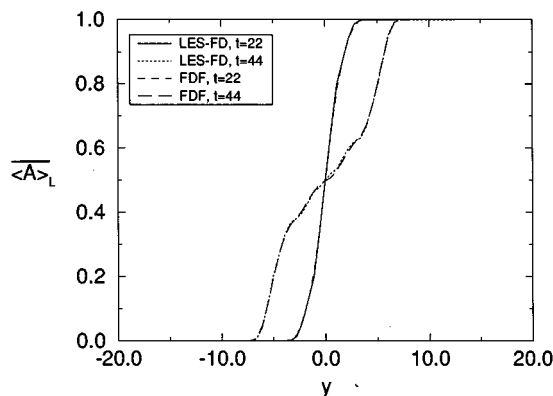


FIG. 8. 3D mixing layer simulation results: Cross-stream variations of the mean value of the filtered mass fraction of a conserved scalar.

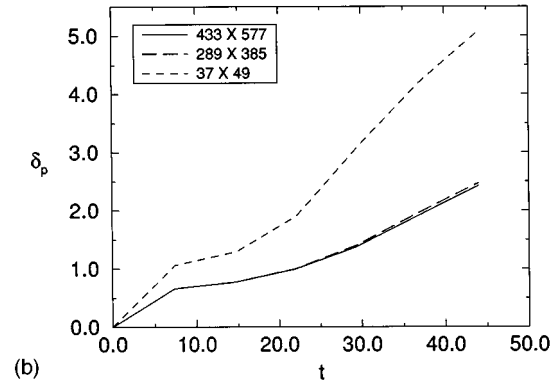
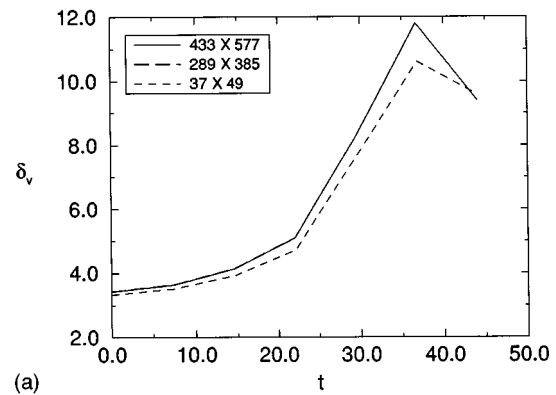


FIG. 9. 2D mixing layer simulation results: Effect of grid resolution on temporal evolution of the (a) vorticity thickness and (b) total product.

First the resolution requirement for DNS is determined. This is demonstrated here for the 2D mixing layer. A similar procedure is followed for the other flow configurations. In Fig. 9 results are presented of the temporal evolution of the vorticity thickness (δ_v) and the total product (δ_p) in a reacting layer with $Re=500$, $Da=2$ at several resolutions. It is shown that the results generated via 289×385 are almost identical to those on 433×577 grid points. Analysis of other statistical results (not shown) show a similar behavior. Hereinafter 433×577 grid points are used in all DNS of the 2D mixing layer. The resolution employed in LES (both FDF

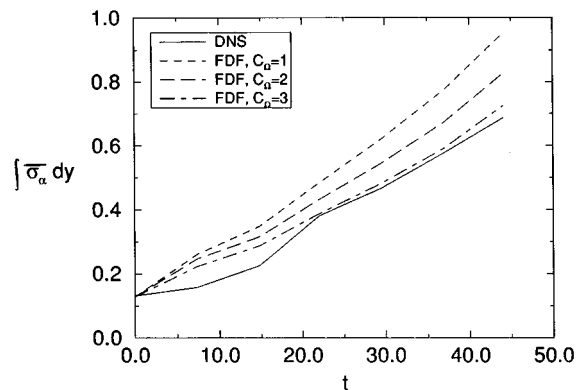


FIG. 10. 2D mixing layer simulation results: The integrated Reynolds averaged values of the filtered scalar's variance vs. time.

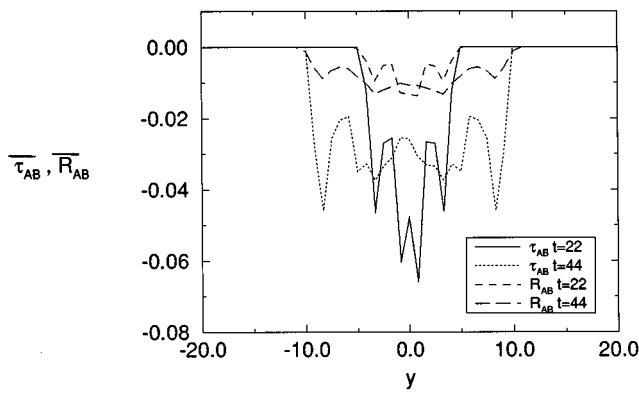


FIG. 11. 2D mixing layer simulation results: Total SGS unmixedness and Reynolds subpart vs. cross-stream coordinate.

and LES-FD) is coarser consisting of 37×49 grid points. The results in Fig. 9 indicate the inaccuracy of “DNS” at this resolution.

To determine the magnitude of C_Ω , in Fig. 10 the integrated Reynolds averaged values of the SGS variance ($\int \overline{\sigma_A}(y,t) dy$) of a nonreacting scalar as predicted by FDF are compared with those via DNS. This comparison shows that $C_\Omega \approx 3$ yields a reasonable agreement between the prediction and DNS results. Thus, this value is used in absence of a better model of the subgrid mixing frequency.

To demonstrate the difficulty of modeling the SGS scalar fluctuations in reacting flows, the Reynolds averaged profiles for the “SGS unmixedness” ($\tau_{AB} = \langle AB \rangle_L - \langle A \rangle_L \langle B \rangle_L$) and its “Reynolds” subpart^{84,85} $R_{AB} = \langle A'B' \rangle_L - \langle A' \rangle_L \langle B' \rangle_L$ as obtained directly from DNS data are shown in Fig. 11. These results show the importance (non-zero values) of these correlations. They also show that R_{AB} is a fraction of τ_{AB} suggesting that modeling of τ_{AB} in LES is more complex than that in Reynolds procedures.

In Fig. 12, the FDF predictions of the total product are compared with DNS results. The Smagorinsky model is employed in FDF with several values of the parameter C_s . Obviously for a constant C_s value, the agreement between DNS and FDF is not very satisfactory. The subgrid viscosity based

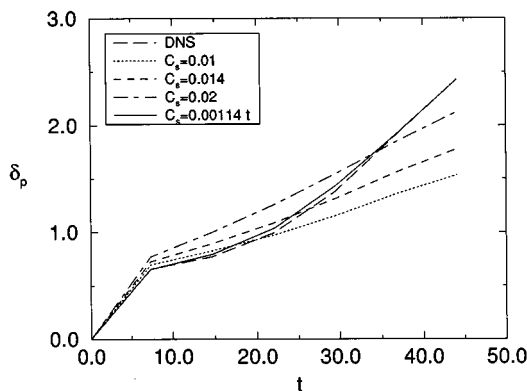


FIG. 12. 2D mixing layer simulation results: Total product variation with time. The Smagorinsky model is used to represent the eddy viscosity for the FDF simulations.

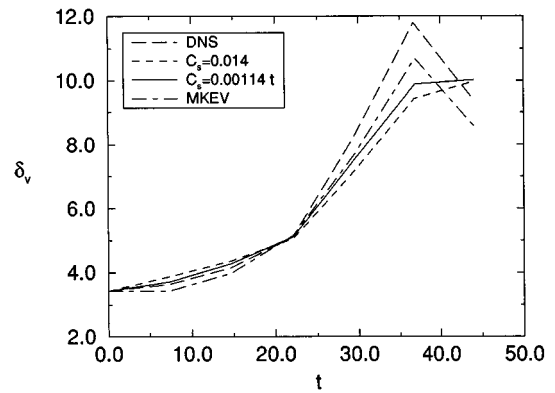


FIG. 13. 2D mixing layer simulation results: Vorticity thickness vs. time.

on the Smagorinsky closure affects both the resolved hydrodynamic field and the subgrid scalar mixing process. It is known that the Smagorinsky closure sometimes generates excessive damping on the resolved scales in transitional regions.⁴⁹ Here, an attempt is made to rectify the situation, albeit in a very *ad hoc* manner. In the temporal mixing later, C_s should be initially zero to reflect the fact that the flow is “laminar.” Then its value should increase in time as the flow becomes more “turbulent.” The FDF results in Fig. 12 with $C_s \propto t$ agree more favorably with DNS. This is partly due to better predictions of the hydrodynamic field (Fig. 13) but also due to more accurate representation of the subgrid mixing frequency. This better agreement is not sufficient to suggest a new model for C_s ; rather it is to demonstrate the importance of the subgrid diffusion in affecting the FDF directly (through the subgrid mixing) and indirectly (through the input of the hydrodynamic parameters).

In order to better predict the subgrid viscosity, the MKEV model (Eq. (11)) is adopted. In Fig. 13 it is shown that the vorticity thickness predicted by the MKEV model compares with DNS data better than that via the Smagorinsky model. The improved prediction of the eddy viscosity also improves the FDF predicted product formation as shown in Fig. 14 for several values of the Damköhler number. Due to the demonstrated superiority, the MKEV closure is utilized in all subsequent simulations unless otherwise noted.

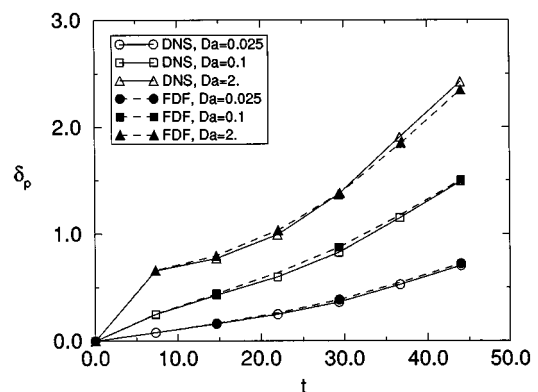


FIG. 14. 2D mixing layer simulation results: Temporal evolution of the total product.

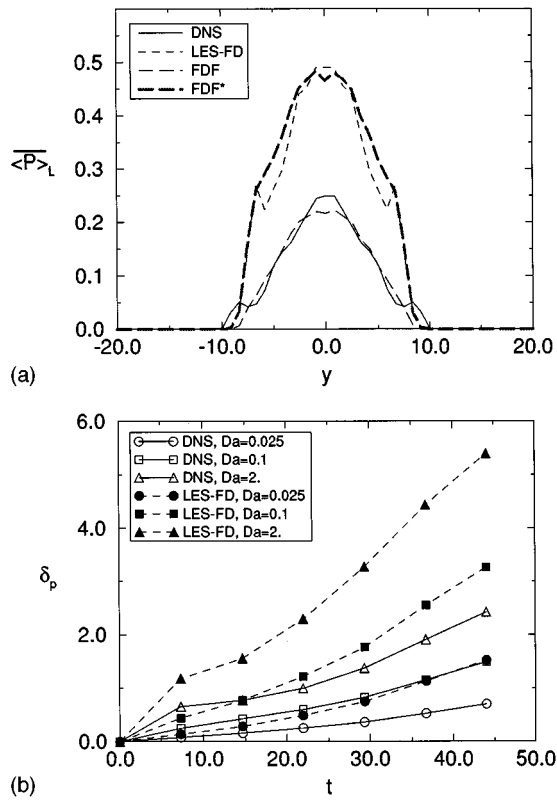


FIG. 15. 2D mixing layer simulation results: (a) Cross-stream variation of the product distribution. (b) Temporal evolution of the total product.

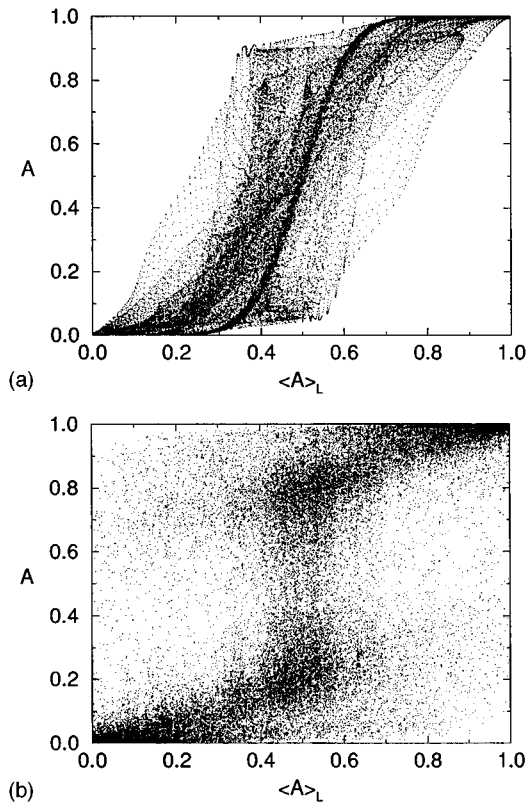


FIG. 16. 2D mixing layer simulation results: Scatter plots of instantaneous value of the conserved scalar vs. the mean value. Data taken from (a) DNS, (b) FDF throughout the computational domain.

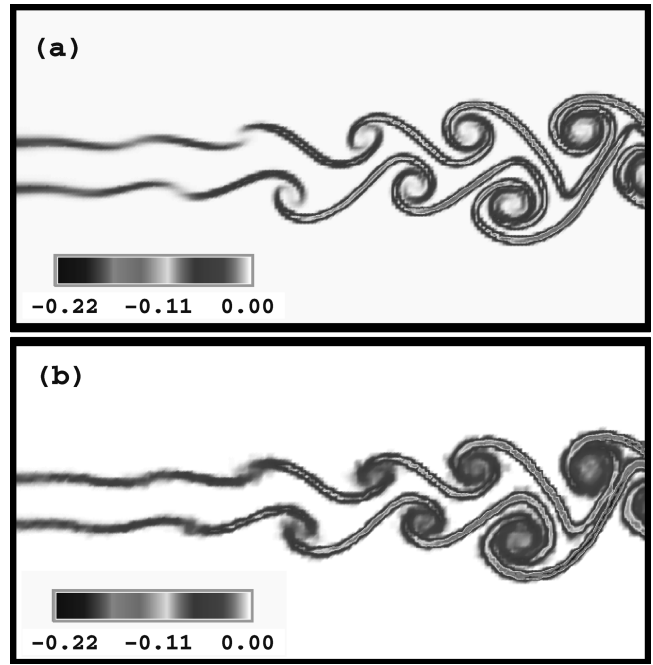


FIG. 17. 2D planar jet simulation results: Contours of the normalized instantaneous subgrid unmixedness (a) DNS, (b) FDF.

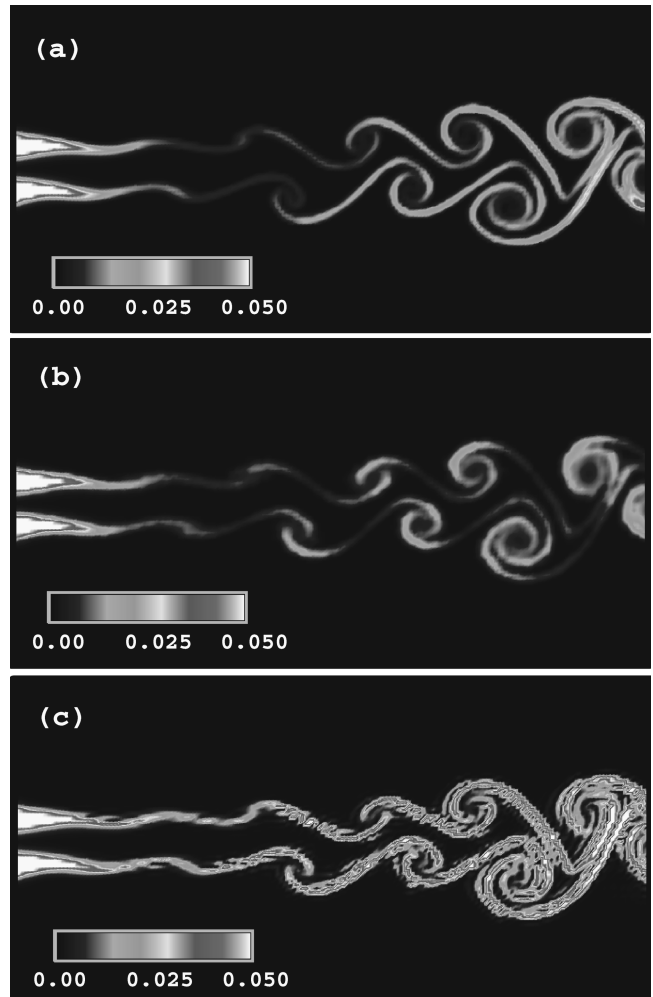


FIG. 18. 2D planar jet simulation results: Instantaneous reaction rate as determined by (a) DNS, (b) FDF, (c) LES-FD.

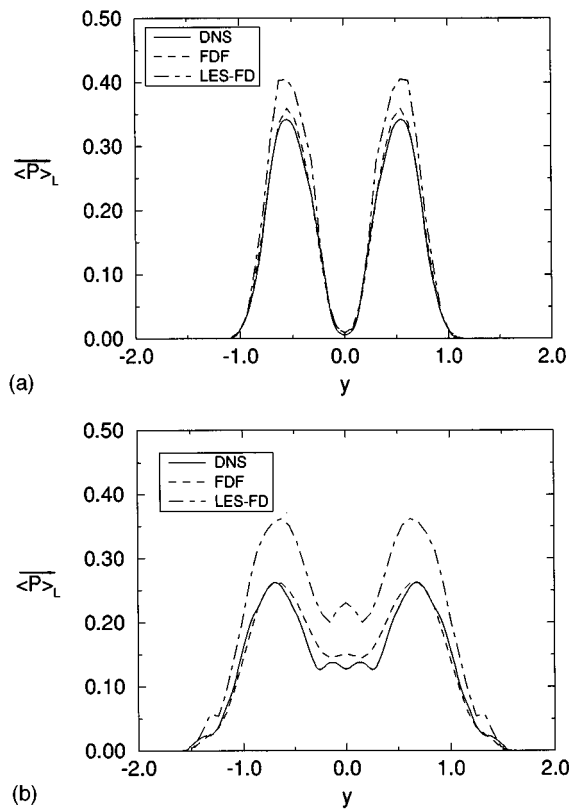


FIG. 19. 2D planar jet simulation results: Cross-stream variation of the mean product mass fraction at (a) $x=5D$ and (b) $x=9D$.

To demonstrate the importance of the SGS scalar fluctuations, the results of FDF and LES-FD are compared with DNS results in Fig. 15. This figure shows that the neglect of SGS unmixedness results in significant overpredictions of the product mass fraction. This behavior is observed at all times and all values of the Damköhler number (Fig. 15(b)) and is consistent with that in Reynolds averaging.¹⁸ Moreover, Fig. 15(b) shows that as the magnitude of the Damköhler number increases, the neglect of the SGS unmixedness in LES-FD results in progressively higher deviation of product formation relative to DNS. This is significant since the Da values in practical reacting systems can be quite

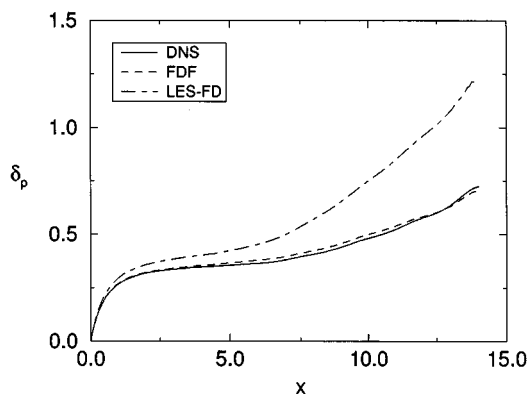


FIG. 20. 2D planar jet simulation results: Total product vs. the downstream coordinate.

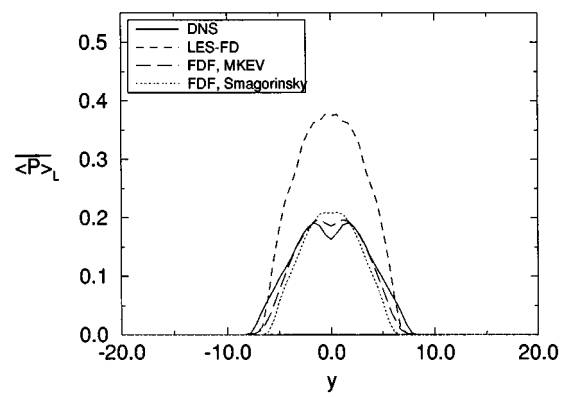


FIG. 21. 3D mixing layer simulation results: Cross-stream variation of the product distribution.

large. Therefore it is expected that the effects of the SGS unmixedness are very pronounced in such applications. To verify that the enhanced product formation in LES-FD is not associated with the numerical discretization errors, an additional FDF is conducted in which the filtered reaction rate is “incorrectly” calculated in terms of the filtered values of the reactants’ mass fractions. The results based on this model are identified by FDF* in Fig. 15(a) and consistent with LES-FD results, overpredict the rate of reactants’ conversion.

It is useful to compare the DNS results for “fine grid” scalar values with the “fine-grained” values associated with the Monte Carlo particles. The “scatter” plots of the instantaneous fine grid values of A vs. its filtered value $\langle A \rangle_L$ as obtained by DNS are presented in Fig. 16(a) and the scatter plot of fine grained A values vs. $\langle A \rangle_L$ is shown in Fig. 16(b). These results are associated with a non-reacting temporal mixing layer and are taken at a fixed time. The points in Fig. 16(a) correspond to the values at all the grid points employed in DNS within the computation domain. The points in Fig. 16(b) correspond to all Monte Carlo particles occupying the same domain. It is shown that the “density” of scatter is similar in the two plots indicating a qualitative agreement between FDF and DNS. However, the scatter in FDF is expectedly somewhat greater but not with a significant density.

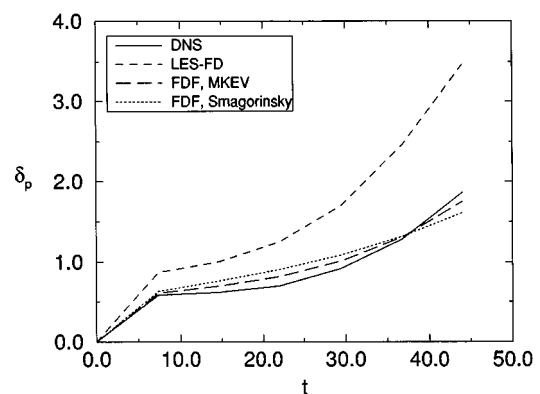


FIG. 22. 3D mixing layer simulation results: Temporal evolution of the total product.

TABLE I. Total computational times for the 2D reacting mixing layer simulations.

Simulation	Grid resolution	NPG	Normalized CPU time ^a	Figure
DNS	433×577	—	285.45	14, 15(b)
FDF	37×49	40	8.45	14
LES-FD	37×49	—	1	15(b)

^aUnit corresponds to 11 s on a Cray-C90.

The effectiveness of the FDF to predict the slightly more complex jet flow is summarized in Figs. 17–20. Figure 17 shows the instantaneous contours of the normalized SGS unmixedness as obtained by filtered DNS and FDF. Note that this term is assumed to be identically zero in LES-FD. The SGS unmixedness is negative throughout the reaction zone, thus its effect is manifested in a decrease of the filtered reaction rate. This is readily observed in Fig. 18, where the contour plots of the reaction rates are displayed for the filtered DNS, FDF and LES-FD approaches. While the peak values in the DNS are slightly higher than those observed in the FDF simulations, the reaction zone predicted by the FDF simulation is slightly thicker (due to the finite size of the ensemble domain) therefore yielding a comparable amount of converted products. In contrast, the filtered reaction rates obtained by the finite difference LES procedure in which the SGS unmixedness is neglected are significantly higher. This is reflected in Fig. 19, where the cross-stream variation of the time-averaged filtered values of the product mass fraction are presented at two downstream locations and in Fig. 20, where the streamwise variation of the integrated total product ($\delta_p(x) = \int \overline{P}_L(x,y) dy$) is shown. Two additional points are intended by presentations of Figs. 19 and 20. First, the FDF results are compatible with those of DNS at all downstream coordinates. Therefore, there is no “secular” behavior associated with possible modeling errors in the FDF. Second, the differences between the FDF and DNS in predicting the subgrid scalar variances at large x/D values as observed in the variance results in Fig. 6 do not seem to yield significant differences in the amount of product formation as predicted by the FDF. In all the cases the neglect of the SGS fluctuations, as done in LES-FD, results in significant overpredictions of the filtered reactant conversion rate. It is expected that these overpredictions would become even more significant at higher Damköhler and Reynolds numbers.

The major conclusions drawn from the 2D results are confirmed in 3D simulations. The cross-stream variation of the filtered mean products and the temporal variation of the total product in the 3D mixing layer are shown in Figs. 21 and 22. The performances of the Smagorinsky and MKEV

TABLE II. Total computational times for the reacting jet simulations.

Simulation	Grid resolution	NPG	Normalized CPU time ^a	Figure
DNS	721×361	—	52.12	18(a)
FDF	181×91	20	12.56	18(b)
LES-FD	181×91	—	1	18(c)

^aUnit corresponds to 809 s on a Cray-C90.

TABLE III. Total computational times for the 3D reacting mixing layer simulations.

Simulation	Grid resolution	NPG	Normalized CPU time ^a	Figure
DNS	217×289×133	—	182.71	21, 22
FDF	55×73×34	20	7.64	21, 22
LES-FD	55×73×34	—	1	21, 22

^aUnit correspond to 655 s on a Cray-C90.

closures in predicting the hydrodynamic field are similar to those in 2D. With either closures, the amount of products predicted by LES-FD is higher than those obtained by FDF and DNS. The FDF results are again in a good agreement with DNS data. This agreement also indicates that the mixing model with $C_\Omega=3$ works well in 3D simulations; no attempt was made to find the optimize value of this constant. Future applications to other flow configurations would determine the generality of the model.

E. Comparison of computational requirements

The total computational times associated with some of the simulations are shown in Tables I–III. The cases considered in this table are those which give reasonably accurate predictions of the first FDF moments of the reacting scalar field. Expectedly, the overhead associated with the FDF simulation is somewhat extensive as compared to LES-FD; nevertheless the FDF’s computational requirement is significantly less than that of DNS. While this overhead was tolerated in present simulations, there are several means of reducing it for future applications. A detailed examination of the individual routines utilized in the FDF simulations indicates that the most demanding computation is associated with the particle interpolation procedure. The fourth order interpolation routine consumes about 51.3% of the total CPU time. The bilinear scheme reduces the computational time by 36%. If interpolation can be totally disregarded, i.e., using the results at the nearest finite difference grid point as shown in Fig. 4, the CPU time can be decreased by 50%. In addition, the Lagrangian procedure would benefit from the utilization of parallel architecture, since a significant portion of the time is devoted to computations in large loops dimensioned by the total number of Monte Carlo particles. This has been discussed for use in PDF (Ref. 86) and its utilization is recommended for FDF.

In comparing the computational requirements of FDF with those of DNS, it is important to note that this comparison could be made only in flows for which DNS was possible. The DNS times and the FDF times are as close as they are simply because the DNS had to be done at low Re , Da values. At higher values of these parameters, the difference could be much greater. This warrants further extensions and applications of FDF for more complex turbulent reacting flows for which DNS is not possible.

VII. CONCLUDING REMARKS

It is demonstrated that the filtered density function (FDF) provides a powerful method for large eddy simulation (LES) of turbulent reacting flows. The method is based on the representation of the distribution of the unresolved fluctuations at the subgrid level. This is similar to the probability density function (PDF) methods in Reynolds averaging procedures. Here, the FDF methodology is developed for treatment of scalar variables. Thus, similar to PDF methods it represents the effects of chemical reactions in a closed form.

A modeled transport equation is developed for the FDF by adopting a closure strategy similar to that in PDF methods. It is shown that the Lagrangian Monte Carlo scheme provides an effective means of solving the FDF transport equation. The scheme is exploited for LES of two- and three-dimensional shear flows under both nonreacting and reacting conditions. The simulated results are compared with those based on conventional LES methods in which the effects of subgrid scalar fluctuations are ignored (LES-FD), and those via direct numerical simulation (DNS) of flows with identical values of the physical parameters. The convergence of the Monte Carlo numerical results and the consistency of the FDF formulation are demonstrated by comparisons with the Eulerian results of LES-FD of non-reacting flows. The superiority of the FDF over LES-FD is demonstrated by detailed comparative assessments with DNS results of reacting shear flows. It is shown that the subgrid scale scalar fluctuations have a very significant influence on the filtered reaction rate; the neglect of these fluctuations results in overpredictions of the filtered reactant conversion rate.

Although the present methodology is developed for isothermal, constant density, reacting flows with a simple kinetics scheme, the extension to variable density flows, with exothermic reactions imposes no serious mathematical difficulties. With such an extension, it is conceivable that LES of reactive flows with realistic chemical kinetics may be conducted for engineering applications in the near future, if the computational overhead associated with the FDF can be tolerated. In this regard, the scalar FDF methodology is attractive in that the present Monte Carlo solver can be used directly in available CFD codes. Similar to PDF methods, the closure problems associated with the FDF are the correlations involving the velocity field (such as SGS stresses and mass fluxes). This may be overcome by considering the joint velocity-scalar FDF similar to that in PDF.⁸⁷

The computational requirement for FDF is more than that for LES-FD and less than that for DNS. The range of flow parameters (such as the Reynolds and the Damköhler numbers) that can be considered by FDF is significantly larger than can be treated by DNS, and the results are more accurate than those by LES-FD. This comparison of computational requirements could be made here only in flows for which DNS was possible, i.e., low Da , Re values. At higher values of these parameters, the computational cost associated with DNS would be exceedingly higher than that of FDF. Thus for practical flows for which DNS is currently impossible, FDF would be a good alternative. Several means of reducing the FDF's computational requirements are recom-

mended. These could be useful in future applications in complex flows. The FDF methodology will benefit from ongoing and future improvements in PDF schemes from both modeling and computational standpoints.⁵⁶

ACKNOWLEDGMENTS

This work is part of a research program sponsored by the NASA Langley Research Center under Grant No. NAG-1-1122 to SUNY-Buffalo and Grant No. NAG-1-1542 to Cornell University. Dr. J. Philip Drummond is the Technical Monitor of this program. Additional support for the work at Cornell is provided by the AFOSR under Grant No. F49620-94-1-0098. Computational resources are provided by the NAS Program at the NASA Ames Research Center and by the SEAS Computing Center at SUNY-Buffalo.

¹J. Smagorinsky, "General circulation experiments with the primitive equations. I. The basic experiment," *Mon. Weather Rev.* **91**, 99 (1963).

²D. K. Lilly, "The representation of small-scale turbulence in numerical simulation experiments," in *Proceedings of the IBM Scientific Computing Symposium Environmental Sciences*, IBM Form No. 320-1951 (1967), pp. 195-210.

³J. H. Ferziger, "Higher level simulations of turbulent flows," Stanford University Report No. TF-16, Department of Mechanical Engineering, Stanford University, Stanford, California, 1981.

⁴P. R. Voke and M. W. Collins, "Large eddy simulation: Retrospect and prospects," *PhysicoChem. Hydrodynam.* **4**, 119 (1983).

⁵R. S. Rogallo and P. Moin, "Numerical simulation of turbulent flow," *Annu. Rev. Fluid Mech.* **16**, 99 (1984).

⁶W.-H. Jou and J. J. Riley, "Progress in direct numerical simulations of turbulent reacting flows," *AIAA J.* **27**, 1543 (1989).

⁷P. Givi, "Model free simulations of turbulent reactive flows," *Prog. Energy Combust. Sci.* **15**, 1 (1989).

⁸*Whither Turbulence? Turbulence at the Crossroads, Lecture Notes in Physics*, edited by J. L. Lumley (Springer, New York, 1990), Vol. 357.

⁹*Numerical Approaches to Combustion Modeling, Progress in Astronautics and Aeronautics*, edited by E. S. Oran and J. P. Boris (AIAA, New York, 1991), Vol. 135.

¹⁰P. A. McMurtry and P. Givi, "Spectral simulations of reacting turbulent flows," in Ref. 9, Chap. 9, pp. 257-303.

¹¹*Large Eddy Simulations of Complex Engineering and Geophysical Flows*, edited by B. Galperin and S. A. Orszag (Cambridge University Press, Cambridge, 1993).

¹²P. Givi, "Spectral and Random vortex methods in turbulent reacting flows," in Ref. 19, Chap. 8, pp. 475-572.

¹³D. K. Lilly, "On the computational stability of numerical solutions of time-dependent non-linear geophysical fluid dynamics problems," *Mon. Weather Rev.* **93**, 11 (1965).

¹⁴M. Germano, "Turbulence: The filtering approach," *J. Fluid Mech.* **238**, 325 (1992).

¹⁵M. Germano, U. Piomelli, P. Moin, and W. H. Cabot, "A dynamic subgrid-scale eddy viscosity model," *Phys. Fluids A* **3**, 1760 (1991).

¹⁶S. B. Pope, "Computations of turbulent combustion: Progress and challenges," in *Proceedings of the 23rd Symposium (International) on Combustion* (The Combustion Institute, Pittsburgh, 1990), pp. 591-612.

¹⁷U. Schumann, "Large eddy simulation of turbulent diffusion with chemical reactions in the convective boundary layer," *Atmos. Environ.* **23**, 1713 (1989).

¹⁸*Turbulent Reacting Flows, Topics in Applied Physics*, edited by P. A. Libby and F. A. Williams (Springer, Heidelberg, 1980), Vol. 44.

¹⁹*Turbulent Reacting Flows*, edited by P. A. Libby and F. A. Williams (Academic, London, 1994).

²⁰W. P. Jones, "Turbulence Modelling and Numerical Solution Methods for Variable Density and Combusting Flows," in Ref. 19, Chap. 6, pp. 309-374.

²¹*Turbulence in Mixing Operation*, edited by R. S. Brodkey (Academic, New York, 1975).

²²H. L. Toor, "The non-premixed Reaction: $A + B \rightarrow$ products," in Ref. 21, pp. 123-166.

- ²³J. C. Hill, "Homogeneous turbulent mixing with chemical reaction," *Annu. Rev. Fluid Mech.* **8**, 135 (1976).
- ²⁴R. S. Brodkey, "Fundamental of turbulent motion," *Chem. Eng. Commun.* **8**, 1 (1981).
- ²⁵P. A. McMurtry, S. Menon, and A. R. Kerstein, "A linear eddy sub-grid model for turbulent reacting flows: Application to hydrogen-air combustion," in *Proceedings of the 24th Symposium (International) on Combustion* (The Combustion Institute, Pittsburgh, 1992), pp. 271–278.
- ²⁶P. A. McMurtry, S. Menon, and A. R. Kerstein, "Linear eddy modeling of turbulent combustion," *Energy Fuels* **7**, 817 (1993).
- ²⁷R. I. Sykes, D. S. Henn, S. F. Parker, and W. S. Lewellen, "Large-eddy simulation of a turbulent reacting plume," *Atmos. Environ.* **26**, 1713 (1992).
- ²⁸T. M. Liou, W. Y. Lien, and P. W. Hwang, "Large-eddy simulations of turbulent reacting flows in chamber with gaseous ethylene injecting through the porous wall," *Combust. Flame* **99**, 591 (1994).
- ²⁹S. Menon, P. A. McMurtry, and A. K. Kerstein, "A linear eddy subgrid model of turbulent combustion," in Ref. 11, Chap. 14, pp. 287–314.
- ³⁰J. P. Boris, F. F. Grinstein, E. S. Oran, and R. L. Kolbe, "New insights into large eddy simulations," NRL Report No. NRL/MR/4400-92-6979, Naval Research Laboratory, Washington, D.C., 1992.
- ³¹C. Fureby and C. Lofstrom, "Large-eddy simulations of bluff body stabilized flames," in *Proceedings of the 25th Symposium (International) on Combustion* (The Combustion Institute, Pittsburgh, 1994), pp. 1257–1264.
- ³²C. Fureby, E. Lundgren, and S. I. Moller, "Large-eddy simulation of combustion," in *Proceedings of the Eighth International Symposium on Transport Phenomena in Combustion*, edited by S. H. Chen (Taylor-Francis, New York, 1996).
- ³³A. W. Cook, J. J. Riley, and G. Kosály, "A laminar flamelet approach to subgrid-scale chemistry in turbulent flows," *Combust. Flame* **109**, 332 (1997).
- ³⁴A. W. Cook, J. J. Riley, and S. M. deBruynKops, "A sub-grid model for nonpremixed turbulent combustion," in *Proceedings of the Eleventh Symposium on Turbulent Shear Flows* (Grenoble, France, 1997), pp. 16.13–16.18.
- ³⁵F. Mathey and J. P. Chollet, "Large eddy simulation of turbulent reactive flows," in *Proceedings of the Eleventh Symposium on Turbulent Shear Flows* (Grenoble, France, 1997), pp. 16.19–16.24.
- ³⁶N. Branley and W. P. Jones, "Large eddy simulation of a turbulent non-premixed flame," in *Proceedings of the Eleventh Symposium on Turbulent Shear Flows* (Grenoble, France, 1997), pp. 21.1–21.6.
- ³⁷H. L. Toor, "Mass transfer in dilute turbulent and nonturbulent systems with rapid irreversible reactions and equal diffusivities," *AIChE J.* **8**, 70 (1962).
- ³⁸S. B. Pope, "The statistical theory of turbulent flames," *Philos. Trans. R. Soc. London* **291**, 529 (1979).
- ³⁹E. E. O'Brien, "The probability density function (PDF) approach to reacting turbulent flows," in Ref. 18, Chap. 5, pp. 185–218.
- ⁴⁰S. B. Pope, "PDF methods for turbulent reactive flows," *Prog. Energy Combust. Sci.* **11**, 119 (1985).
- ⁴¹C. Dopazo, "Recent Developments in PDF Methods," in Ref. 19, Chap. 7, pp. 375–474.
- ⁴²T. S. Lundgren, "Distribution functions in the statistical theory of turbulence," *Phys. Fluids* **10**, 969 (1967).
- ⁴³C. K. Madnia and P. Givi, "Direct numerical simulation and large eddy simulation of reacting homogeneous turbulence," in Ref. 11, Chap. 15, pp. 315–346.
- ⁴⁴A. W. Cook and J. J. Riley, "A subgrid model for equilibrium chemistry in turbulent flows," *Phys. Fluids* **6**, 2868 (1994).
- ⁴⁵S. H. Frankel, V. Adumitroaie, C. K. Madnia, and P. Givi, "Large eddy simulations of turbulent reacting flows by assumed PDF methods," edited by S. A. Ragab and U. Piomelli, *Engineering Applications of Large Eddy Simulations* (ASME, New York, 1993), Vol. 162, pp. 81–101.
- ⁴⁶F. Gao and E. E. O'Brien, "A large-eddy simulation scheme for turbulent reacting flows," *Phys. Fluids A* **5**, 1282 (1993).
- ⁴⁷A. A. Aldama, "Filtering techniques for turbulent flow simulations," *Lecture Notes in Engineering* (Springer, New York, 1990), Vol. 49.
- ⁴⁸B. Vreman, B. Geurts, and H. Kuerten, "Realizability conditions for the turbulent stress tensor in large-eddy simulation," *J. Fluid Mech.* **278**, 351 (1994).
- ⁴⁹T. A. Zang and U. Piomelli, "Large eddy simulation of transitional flow," in Ref. 11, Chap. 11, pp. 209–227.
- ⁵⁰R. M. Kerr, J. A. Domaradzki, and G. Barbier, "Small-scale properties of nonlinear interactions and subgrid-scale energy transfer in isotropic turbulence," *Phys. Fluids* **8**, 197 (1996).
- ⁵¹J. Bardina, J. H. Ferziger, and W. C. Reynolds, "Improved turbulence models based on large eddy simulations of homogeneous, incompressible, turbulent flows," Department of Mechanical Engineering Report No. TF-19, Stanford University, Stanford, California, 1983.
- ⁵²T. M. Eidson, "Numerical simulation of the turbulent Rayleigh-Benard problem using subgrid modelling," *J. Fluid Mech.* **158**, 245 (1985).
- ⁵³C. Dopazo and E. E. O'Brien, "Statistical treatment of non-isothermal chemical reactions in turbulence," *Combust. Sci. Technol.* **13**, 99 (1976).
- ⁵⁴R. Borghi, "Turbulent combustion modeling," *Prog. Energy Combust. Sci.* **14**, 245 (1988).
- ⁵⁵S. B. Pope, "A Monte Carlo method for the PDF equations of turbulent reactive flow," *Combust. Sci. Technol.* **25**, 159 (1981).
- ⁵⁶S. B. Pope, "Lagrangian PDF methods for turbulent flows," *Annu. Rev. Fluid Mech.* **26**, 23 (1994).
- ⁵⁷A. J. Chorin and J. E. Marsden, *A Mathematical Introduction to Fluid Mechanics* (Springer, New York, 1979).
- ⁵⁸A. Leonard, "Vortex methods for flow simulation," *J. Comput. Phys.* **37**, 289 (1980).
- ⁵⁹A. Majda, "Vortex dynamics: Numerical analysis, scientific computing, and mathematical theory," in *ICIAM '87*, edited by J. McKenna and R. Temam (Society for Industrial and Applied Mathematics, Philadelphia, 1988), pp. 153–182.
- ⁶⁰T. Sarpkaya, "Computational methods with vortices—The 1988 Freeman Scholar Lecture," *J. Fluids Eng.* **111**, 5 (1989).
- ⁶¹A. F. Ghoniem, "Vortex simulation of reacting shear flow," in Ref. 9, Chap. 10, pp. 305–348.
- ⁶²*Vortex Methods and Vortex Motion*, edited by K. E. Gustafson and J. A. Sethian (SIAM, Philadelphia, 1991).
- ⁶³H. Risken, *The Fokker-Planck Equation, Methods of Solution and Applications* (Springer, New York, 1989).
- ⁶⁴C. W. Gardiner, *Handbook of Stochastic Methods* (Springer, New York, 1990).
- ⁶⁵S. Karlin and H. M. Taylor, *A Second Course in Stochastic Processes* (Academic, New York, 1981).
- ⁶⁶E. E. Kloeden and E. Platen, *Numerical Solution of Stochastic Differential Equations, Applications of Mathematics, Stochastic Modelling and Applied Probability* (Springer, New York, 1995), Vol. 23.
- ⁶⁷P. Billingsly, *Probability and Measure* (Wiley, New York, 1979).
- ⁶⁸E. Helfand, "Numerical integration of stochastic differential equations," *Bell Syst. Tech. J.* **58**, 2289 (1979).
- ⁶⁹D. T. Gillespie, *Markov Processes, An Introduction for Physical Scientists* (Academic, New York, 1992).
- ⁷⁰K. Itô, *On Stochastic Differential Equations, Memoirs of the American Mathematical Society* (American Math Society, Providence, 1951), Vol. 4.
- ⁷¹I. I. Gikhman and A. V. Skorokhod, *Stochastic Differential Equations* (Springer, New York, 1972).
- ⁷²M. H. Carpenter, "A high-order compact numerical algorithm for supersonic flows," in *Proceedings of the Twelfth International Conference on Numerical Methods in Fluid Dynamics, Lecture Notes in Physics*, edited by K. W. Morton (Springer, New York, 1990), Vol. 371, pp. 254–258.
- ⁷³R. W. MacCormack, *The Effect of Viscosity in Hypervelocity Impact Catering*, AIAA Paper 69-354, 1969.
- ⁷⁴J. J. Riley, R. W. Metcalfe, and S. A. Orszag, "Direct numerical simulations of chemically reacting mixing layers," *Phys. Fluids* **29**, 406 (1986).
- ⁷⁵J. J. Riley and P. A. McMurtry, "The use of direct numerical simulation in the study of turbulent chemically reacting flows," edited by R. Borghi and S. N. B. Murthy, *Turbulent Reactive Flows*, Lecture Notes in Engineering (Springer, New York, 1989), pp. 486–514.
- ⁷⁶P. Givi and J. J. Riley, "Some current issues in the analysis of reacting shear layers: Computational challenges," edited by M. Y. Hussaini, A. Kumar, and R. G. Voigt, *Major Research Topics in Combustion*, (Springer, New York, 1992), pp. 588–650.
- ⁷⁷P. A. McMurtry and P. Givi, "Direct numerical simulations of a reacting, turbulent mixing layer by a pseudospectral-spectral element method," edited by T. J. Chung, *Finite Elements in Fluids* (Hemisphere, Washington, D.C., 1992), Chap. 14, pp. 361–384.
- ⁷⁸C. J. Steinberger, T. J. Vidoni, and P. Givi, "The compositional structure and the effects of exothermicity in a nonpremixed planar jet flame," *Combust. Flame* **94**, 217 (1993).
- ⁷⁹R. D. Moser and M. M. Rogers, "Mixing transition and the cascade of small scales in a plane mixing layer," *Phys. Fluids A* **3**, 1128 (1991).

- ⁸⁰R. S. Miller, C. K. Madnia, and P. Givi, "Structure of a turbulent reacting mixing layer," *Combust. Sci. Technol.* **99**, 1 (1994).
- ⁸¹G. Erlebacher, M. Y. Hussaini, C. G. Speziale, and T. A. Zang, "Toward the large eddy simulation of compressible turbulent flows," *J. Fluid Mech.* **238**, 155 (1992).
- ⁸²L. Arnold, *Stochastic Differential Equations: Theory and Applications* (Krieger, Malbar, 1974).
- ⁸³T. T. Soong, *Random Differential Equations in Science and Engineering* (Academic, New York, 1973).
- ⁸⁴A. Leonard, "Energy cascade in large-eddy simulations of turbulent flows," *Adv. Geophys.* **18A**, 237 (1974).
- ⁸⁵M. Germano, "A proposal for a redefinition of the turbulent stresses in the filtered Navier-Stokes equations," *Phys. Fluids* **29**, 2323 (1986).
- ⁸⁶A. D. Leonard and F. Dai, "Applications of a coupled Monte Carlo PDF/finite volume CFD method for turbulent combustion," AIAA Paper No. 94-2904, 1994.
- ⁸⁷S. B. Pope, "On the relation between stochastic Lagrangian models of turbulence and second-moment closures," *Phys. Fluids* **6**, 973 (1994).